Evidence for Active Hotspots on Venus from Analysis of Magellan Gravity Data

Suzanne E. Smrekar
Jet Propulsion Laboratory
MS 183-501
4800 oak Grove Dr.
Pasadena, CA 91209

tel: 818-354-4192
fax: 818-393-5059
e-mail: ssmrekar@cytherа.jpl.nasa.gov

number of pages: 43
number of figures: 13 numbered, 31 total
number of tables: 1
key words: Venus, hotspot, gravity, Magellan, elastic thickness
Submitted to Icarus: March 3, 1993

Running header:

EVIDENCE FOR ACTIVE HOTSPOTS ON VENUS

Correspondence:

Suzanne E. Smrekar
Jet Propulsion Laboratory
MS 183-501
4800 Oak Grove Dr.
Pasadena, CA 912.09
tel: 818-354-4192
fax: 818-393-5059
e-mail: ssmrekar@cythera.jpl.nasa.gov

ABSTRACT

The 500 My average crater retension for Venus has raised questions about the present-day level of tectonic activity. In this study we examine the relationship between the gravity and topography of four large volcanic swells, Beta, Atla, Bell, and Western Eistla Regiones, for clues about their stage of evolution. The Magellan line-of-sight gravity data is inverted using a point mass model of the anomalous mass to solve for the local vertical gravity field. Spectral admittance calculated from both the local gravity inversions and a spherical harmonic model are compared to three models of compensation: local compensation, a 'flexural' model with local and regional compensation of surface and subsurface loads, and a 'hotspot' model of compensation that includes top loading by volcanoes and subsurface loading due to a deep, low density mass anomaly. The coherence is also calculated in each region, but yields an elastic thickness estimate only at Bell Regio. Both local and regional compensation are evident in each area, In all models, the long wavelengths are. compensated locally. The long wavelength estimates of the deep compensation depth for Bell, Atla, Western Eistla, and Beta Regiones are 125, 175,200, and 225 km, respectively, with an error of approximately ± 35 km. "l'he flexural model is rejected primarily because it gives values of effective elastic thickness of approximately 100 km, which is at least a factor of two larger than estimates of effective elastic thickness obtained from the coherence spectra at Bell Regio and from other studies that model the topographic expression of flexure at Bell Regio and in other tectonic settings globally. Assuming a crustal thickness of 30 km, the fit to the hotspot model at Atla Regio gives an effective elastic thickness of 30±5 km, Atla Regio is interpreted as an active hotspot because of the deep compensation depth and a strong subsurface loading signature. At Bell Regio, effective elastic thickness is 30±5 km at short wavelengths and 50±5 km at long wavelengths, using a crustal thickness of 10 km. The 30 km value is interpreted as the effective elastic thickness at the time when the volcanoes are implaced; the S() km value is believed to reflect the present-day effective elastic thickness. Bell Regio has a relatively shallow compensation depth,

125 km, and a weak bottom-to-top loading ratio determined from the coherence spectra. These results may indicate a relatively old, possibly inactive plume, The data at Beta and Western Eistla Regiones are of relative] y poor quality and do not permit detailed interpretations. These areas are interpreted as active hotspots because. of their large compensation depths, greater than typical of the rest of the planet.

INTRODUCTION

I arge volcanic swells were first identified on Venus in the Pioneer Venus radar, altimetry and gravity data. Numerous highlands were interpreted to be analogous to terrestrial hotspots on the basis of their broad topographic swells, evidence for extension, abundant volcanism, including major volcanic edifices, and their large positive gravity anomalies (Phillips *et al. 1981;* McGill *et al.* 1981; Esposito *et al.* 1982; Morgan and Phillips 1983; Phillips and Malin 1983, 1984). in particular, their large positive gravity anomalies have been used to argue that these areas represent active mantle plumes (Phillips et *al. 1981;* Esposito *et al.* 1982; Phillips and Malin 1983, 1984, Janale *et al. 1987;* Smrekar and Phillips 1991; Kiefer and Hager 1991; Black *et al. 1991;* Grimm and Phillips 1992; Binschadler *et al. 1992).* The improved resolution and quality of the Magellan gravity data (Konopliv anti Sjogren 1994), along with analysis of Magellan radar images and topography data in these regions (Stofan *et al. 1994),* provide an important opportunity to better characterize the nature of compensation and evolution of these large topographic swells.

Studies of Magellan data also provides a new context for the study of hotspots on Venus. High resolution, global radar coverage confirm that there maybe local regions of plate boundaries (McKenzie *et al.* 1992), but that terrestrial style plate tectonics is absent on Venus (Solomon *et al. 1992.).* This finding reaffirms the important role of hotspots as a window to mantle convection on Venus. Perhaps the most startling result from Magellan data analysis is the average crater retension age of 500 My coupled with the observation that only -5% of the craters are modified (Schaber *et al. 1992;* Phillips *et al. 1992).* Two end-member models arc consistent with these finding. In one model, the planet was complete] y resurfaced 500 Ma and has been generally inactive since then (Schaber *et al.* 1992; Phillips *et al.* 1992). in the other extreme, the planet is continuously resurfacing at an average, steady rate, with resurfaced areas confined to being smaller than typical intracrater distances (Phillips *et al,* 1992). ongoing studies of the impact cratering record suggest that the true history of resurfacing on Venus is

probably intermediate between these models. The presence of active hotspot on Venus would clearly argue for some level of ongoing resurfacing.

A key to determining the role of hotspots in both the heat loss and the resurfacing, history of Venus is an understanding of their evolution. Both the heat loss and amount of volcanism reaching the surface changes over the life time of the plume. Numerical models and laboratory experiments predict the time evolution of the topography, gravity, and volcanism due to rising mantle plumes (Olsen and Nam 1986; Griffiths *et al.* 1989; Griffiths and Campbell 1991; Bindschadler and Parmentier 1990; Manga *et al, 1993;* Moresi and Parsons 1994; Smrekar and Parmentier 1994). The greatest compensation depth occurs when the plume is still quite deep in the mantle. As the plume approaches the surface and flattens out, the compensation depth decreases. These studies predict that a significant amount of uplift should occur prior to pressure release melting and that rifting should occur prior to the formation of volcanic edifices.

By studying all possible hotspot canidates, it may be possible to distinguish between the effects of evolutionary stage and differences in the size and magnitude of a plume or of variations in the properties of the lithosphere. In addition to thermal buoyancy, lateral viscosity variations (Moresi and Parsons 1994) and chemical density differences related to pressure release melting (Smrekar and Parmentier 1994) also affect the evolution of gravity and topography above a plume. Both effects tend to give a deeper apparent depth of compensation. Thus all variations in apparent depth of compensation may not be directly related to the depth of the plume head. For this reason, we do not try to distinguish a 'dynamic' signature in the gravity, due to viscous forces rather than density differences. In this study, an active hotspot is defined as a region which has the general characteristics of hotspots and in which there is evidence for a thermal anomaly at depth.

The goals of this study are to evaluate the evidence for active plumes on Venus using the new Magellan gravity data, to utilize the higher data resolution to constrain not only the compensation mechanism but also the effective elastic thickness in these regions, and to use this information to try to understand the evolutionary stage of each hotspot examined. We

investigate the gravity and topography fields for four large volcanic swells identified as probable hotspots: Beta, Atla, Bell, and Western Eistla Regiones. These regions were selected both because of the low altitude Magellan gravity data coverage already available and because of their large size and thus relatively important role in venusian tectonics.

Below we describe the characteristics of the four regions, the Magellan gravity and topography data sets, and the method of local point mass inversion used in this study to obtain vertical gravity maps of each area, The spectral admittance, or the ratio of gravity-to-topography as a function of wavelength, is calculated for each region using the gravity from both the regional inversions and a spherical harmonic field (Konopliv and Sjogren 1994) and compared with three different models of compensat ion. The first model is local, isostatic compensation, due to either an Airy or Pratt mechanism, the second includes the effects of surface and subsurface loading as well as local compensation (Forsyth 1985), and the third is specific to the hotspot environment (McNutt and Shure 1986), utilizing the observation that volcanic edifices load the plate from above and the assumption that a low density, thermal anomaly loads the plate from below.

BRIEF GEOLOGIC DESCRIPTION

The four volcanic swells examined here are Beta, Atla, Bell, and Western Eistla Regiones have all been described in detail, on the basis of Pioneer Venus, Arecibo, and Magellan data (McGill *et al.* 1981; Campbell *et al.* 1984; Stofan *et al. 1989,* Senske et *al.* 1992; Grimm and Phillips 1992). Swell and volcanic edifice dimensions are given in Stofan et al. (1994). Each region has its unique characteristics. Bell Regio is among the smallest of the volcanic swells and has two distinct topographic highs (Fig 1). The volcanic edifice, Tepev Mons, is one of the few volcanoes on Venus that has a clear topographic moat. McGovern and Solomon (1992) find a best fitting effective elastic thickness of 10-20 km at Tepev Mons. Two large coronae are also located on the flanks of Bell Regio (Fig. 1). The only evidence for extension is a few

small graben near the center of the swell. Atla Regio has three major volcanic edifices, including Maat Mons, which is over 9 km high (Fig. 2). Both Maat and Ozza Montes have complex systems of fractures and flows. Both Beta and Atla Regiones have extensive arrays of wide (up to 200 km across), deep (up to 2 km) rifts (Solomon *et al. 1992).* These huge rift systems that cross Atla and Beta Regiones are continuous with an equatorial extension belt (Schaber *et al.* 1982) and thought to be too large to be the result of topographic uplift alone (Stofan et *al. 1989).* Volcanism in these rifts in the area of Atla and Beta Regiones is minimal (Senske *et al.* 11992; Solomon *et al. 1992).* Of all the volcanic rises, Western Eistla Regio is the most similar to terrestrial swells in that it has a relatively simple swell geometry with two volcanic edifices, Sif and Gula Montes, near the top of the swell (Fig. 3). It has a relatively minor rift system, Guor Linea (Grimm and Phillips 1992; Solomon *et al. 1992).* Two large corona occur on the northern flank of the swell. Beta Regio was the first large volcanic swell (Fig. 4) to be identified and characterized as a possible hotspot (McGill *et al.* 198 1; Esposito *et al. 1982).* It is unusual in that it is dominated by large regions of complex ridged, or tessera, terrain (Senske *et al.* 1992) and has the largest gravity -to-topography ratio, or apparent compensation depth, of any of the swells (Smrekar and Phillips 1991; Simons *et al.* 1994). The one major volcanic edifice is Theia Mons (Fig. 4).

DATA

The data sets used in this study are derived from Magellan radar altimetry and line-of-sight (LOS) gravity data. The Magellan topography data set used is the global topography data record, a Cartisan representation of the topography (Ford and Pettengill 1992), averaged to 10 bins. Gravity data is primarily collected using X- bane] radar frequency, giving Magellan data a significantly higher signal-to-noise ratio (Sjogren and Phillips 1994). This translates into a data error of less than 0.5 mgals versus 1-2 regal data error in the Pioneer Venus data (Sjogren *et al., 1980).* Over the regions examined, the Magellan spacecraft altitude varied from

approximately 160 km to 430 km. Since the. four regions are at low latitude, this altitude range is similar to that of Pioneer Venus. LOS gravity data is determined by measuring the change in the doppler shift of the radar communications signal along the line between the spacecraft and Earth and removing all known influences on the spacecraft motion (Phillips et *al.* 1978). Since Earth, the spacecraft and Venus seldom lie exactly along a line, the LOS data contain both vertical and horizontal components of gravity, making it necessary to go though an inversion process to extract the vertical gravity data before detailed interpretation. The line-of-sight angle is defined as the angle between the Earth, Venus and the spacecraft. A 0° angle is the best viewing geometry, a 90° angle is the worst, In this study we use both vertical gravity data from a global spherical harmonic model (Konopliv and Sjogren 1994) and from local inversions for vertical gravity. 'I'he inverse method is described below.

There are several reasons for using two types of gravity models for each region. Once produced, the spherical harmonic data set provides a more convenient data set for looking at gravity and topography than doing local inversions over each region. The global models more accurately model the very long wavelength portion of the gravity field and can be easily filtered to remove wavelengths longer than those in the study region or to emphasize certain features. However, presently, the resolution of the spherical harmonic models is only degree and order 60, which corresponds to a wavelength of 630 km. Local gravity inversions are able to obtain a resolution of 300-400 km in certain regions of high data quality and large gravity anomalies. In some cases, this increased resolution is critical for trying to determine the effective elastic thickness of the lithosphere, as discussed below. Comparison of the two methods provides a useful check on the validity of the solutions.

METHODOLOGY

Local Inversion for Vertical Gravity

We invert the 1.0S data using a singular value decomposition method to obtain a point mass representation of the anomalous mass. The form of the generalize linear inverse problem is Ax = y, where x is a vector containing the point masses, y is a vector containing the observed LOS accelerations, and A is a matrix containing the partial derivatives, $\partial y_i/\partial x_j$, of the m accelerations with respect to the n point masses. The partial derivative matrix , A, *is* obtained by using the GASP program (Grimm *et al. 1994),* which is similar to the ORB S1 M program (Phillips *et al.* 1978), to calculate the attraction at each observation site for each of the point masses, using a unit mass. The orbit simulation accounts for the affect of the point masses on the spacecraft orbit, in addition to the standard perturbations. This type of approach, which includes the effect of the anomalous mass on the spacecraft is known as a dynamic method. Each model converges in one iteration using the full rank solution. A grid of point masses is arranged in a grid at 10 intervals at each location. The grid extends out 5° beyond the final region of interest to take into account any effects on the spacecraft arising from anomalous mass beyond the borders of the study area. Table 1 gives the latitude, longitude coordinates of the each inversion, the number of point masses in the grid, the number of singular values retained in the solution (see below), the number of orbits used, the range of orbit numbers, and the number of observations.

The optima] singular value decomposition solution to the inverse problem is selected by evaluating the trade-off between resolution and model error as a function of the number of singular values retained in the solution. "l'he resolution is better when more singular values, which correspond to the point masses, are retained. I lowever, the increase in resolution of the model is accompanied by an increase in model error. This trade off between error and resolution is illustrated for the local inversion at Bell Regio in Fig. 5a, The model covariance

for a singular value decomposition solution is given by $(cov\ x) = \sigma_d^2 A^{-g} A^{-gT}$ where σ_d is the variance of the data, A^{-g} is the inverse (-g indicates a generalized inverse), and T denotes the transpose of the matrix (Menke 1984). An additional check on the choice of singular value is to examine the minimum and maximum values of the gravity field, at a particular altitude, as a function of the number of singular values retained in the solution. In many cases, there is a range of singular value cut off where there is little variation in the minimum and maximum gravity signal, indicating that the full resolution of the data is being modeled without introducing noise from unconstrained point masses (Fig. 5b). Finally, a visual inspection of the gravity map should verify that no unconstrained point masses are included, by making sure that no spurious 'bull's eyes' or undulations at the spacing of point masses are apparent.

The appropriate choice of singular value cut off is a function of the altitude at which the gravity field is calculated, since the altitude affects the resolution, The higher the altitude, the lower the resolution and the greater the number of singular values that can be retained in the solution. Gravity fields for the four regions studied here are calculated at approximately the average value of the spacecraft altitude, at 200 or 2S0 km.

Analysis

The emphasis in this paper is on analysis in the spectral domain, which is advantageous for several reasons. Analyzing the data as a function of wavelength can reveal the presence of multiple compensation mechanisms and provide constraints on the effective elastic thickness. Approaches that find the geoid-to-topography ratio or an apparent depth of compensation can be biased by the presence of multiple compensation mechanisms. Spectral coherence, which gives a measure of the statistical relationship between gravity and topography, gives the most reliable estimate of flexural thickness possible from gravity data (Forsyth 1985). Further, spectral techniques can accommodate minor phase differences between the gravity and topography data sets (illustrated below) more readily that spatial domain analyses.

The spectral admittance approach is fully described by Dorman and Lewis (1970) and has been used determine the compensation depths and effective elastic thickness of numerous terrestrial environments (e.g. McKenzie and Bowin 1976; McNutt 1983), including hotspots (McNutt and Shore 1986; Fischer *et al.* 1986; McNutt 1988; Filmer and McNutt 1988; Sheehan and McNutt 1989). This approach assumes that the relationship between gravity and topography is both linear and isotropic, Uncorrelated parts of the signals are assumed to be noise. The admittance function is defined as cross spectrum of the gravity and over the power spectrum of the topography

$$Z = \frac{\mathrm{Re} \langle G \cdot H^* \rangle}{\langle H \cdot H^* \rangle} \tag{1}$$

where k is the wavenumber, equal to 2n/wavelength, the angular brackets denote averaging over discrete wavenumber bands, G(k) is the Fourier transform of the gravity, $H(k)$ is the Fourier transform of the topography, *Re* indicates the real part of the Fourier transform, and * indicates the complex conjugate (e.g. McNutt 1979). The gravity and topography data are mirrored prior to taking the Fourier transform to minimize edge effects (McNutt 1983). "l'he uncertainty in each estimate of ∂Z_n is given by

$$\partial Z = \frac{(\langle G - Z]] \rangle \ \langle G^* - Z H^* \rangle)^{1/2}}{(\langle H \cdot H^* \rangle)^{1/2}} \tag{2}$$

in this paper, we define the coherence in terms of the Fourier transform of the Bouger gravity (the observed gravity minus the gravity predicted by the topography), B

$$c_o^2 = \frac{\langle BH^* \rangle^2}{\langle BB^* \rangle^2 \ \langle HH^* \rangle^2} \tag{3}$$

For n discrete wavenumbers in a wavenumber band, an unbiased coherence value can be obtained when there is noise in the data (Munk and Cartwright 1966) from

$$c^2 = \frac{n c_o^2 -]}{n-1} \tag{4}$$

The standard deviation in the coherence (Bendat and Piersol 1980) is calculated as

$$\Delta c^2 = (1 - c_o^2)(2c_o^2/n)^{1/2} \tag{5}$$

Compensation Mode/s. The primary goals of the modeling the admittance are to estimate the effective elastic thickness at the time of loading and to determine the compensation depths of the broad swells. The interpretation of gravity data is always non-unique in the absence e of significant additional constraints. For this reason, we fit three different compensation models to the data in each of the four regions. The simplest model is local, isostatic compensation, either Airy or Pratt. The second model, referred to as the flexural model, includes the effects of both surface and subsurface loading of the elastic lithosphere. The third model, the hotspot model, takes advantage of the loading geometry specific to hotspots (McNutt and Shore 1986), and is described below.

Surface and subsurface loading produce very different gravity signatures at short wavelengths (Forsyth 1985), where the exact wavelength at which the difference becomes apparent is a function of the effective elastic thickness. The predicted admittance for a thin elastic plate loaded from above is

$$Q_t(k) = -2\pi\rho_0 G \exp(-kz_m) / (1 + Dk^4/\Delta\rho g) \quad (6)$$

where G is the gravitational constant, equal to $6.673 \times 10^{-11} Nm^2kg^{-2}$, z_m is the depth to the density contrast, which is typically the crust-mantle interface, D is the flexural rigidity of the plate, Ap is the density contrast between the crust (p.) and mantle (ρ_m), taken as 2900 and 3300 kg/m^3, respectively, and g is acceleration of gravity, 8.87 ms^{-2} at the surface of Venus. The flexural rigidity, D, is defined as $ET_e/12(1 - \nu^2)$, where E is the Young's modulus, v is Poisson's ratio, taken as 10^{11} Pa and 0.25, respectively, and Te is the effective elastic thickness of the elastic plate. For isostatic compensation, D is zero, and Eq. 9 reduces to $Q_t(k) = -2\pi\rho_0 G \exp(-kz)$. Although this admittance equation is phrased in terms of Airy compensation, Pratt compensation has the same form. To interpret compensation depths as Pratt compensation rather than Airy compensation, z must be multiplied by a factor of 2 due to the lower thermal density contrast.

Over the wavelength range where flexure is important, the predicted admittance curve due to bottom loading, has a very different shape from top loading since the effect of the elastic plate is to resist the upwarp of the topography rather than the downwarp caused by top loading (Forsyth 1985). In this case, the admittance is directly proportional to D, rather than inversely proportional

$$Q_b(k) = -2\pi G \exp(-kz_m)(1 + Dk^4/\rho_0 g) \quad (7)$$

If both bottom and top loading are present, the admittance curve will be intermediate bet ween the bottom and top loading models (Forsyth 1985). The exact shape of the curve will be determined by f, the ratio of bottom to top loading

$$f = \frac{\xi \Delta\rho |H_B|}{\rho_0 |H_T|} \quad (8)$$

where 1 H_B and H_T are the amplitudes of surface deflection produced by bottom and top loading, respectively (Forsyth 1985).

The final model we consider is the "hotspot" model, developed by McNutt and Shure (1986). This linear filtering approach takes advantage of the loading geometry specific to many hotspots. Typically large shield volcanoes with diameters on the order of hundreds of kilometers load the elastic plate. from above from above and cause downwarp of the crust-mantle boundary, as described in Eq. 6. Thus at short wavelengths, the admittance spectra should be dominated by a top loading signature. At the scale of the broad topographic swell, the crust-mantle boundary is upwarped by the viscous and buoyancy forces due to mantle plume and the elastic plate is loaded from below. The plume forces, which are dominated by a low density thermal anomaly at some depth beneath the crust, supplies an additional compensation interface. These factors combine to give a very different signature at long wavelengths. For Venus, where there is no ocean, the long wavelength, or “swell” portion of the admittance has the form

$$F'_s = 2\pi G\left\{(\rho_m-\rho_o)\exp(-kz_m) + \frac{(\rho_o)}{1+k^4\alpha}\exp(-kz_m)\right.$$

$$\left. - \left((\rho_m + \alpha k^4(\rho_m-\rho_o)\ )\exp(-kz_l)\right)\right\} \qquad (9)$$

$$\alpha = \frac{D}{(\rho_m-\rho_o)g}$$

The first term applies the correct sign to the density contrast to describe upwarp of the crust-mantle boundary, the second term undoes the effects of top loading, and the third term describes the bottom loading and density contrast due to a deep (presumably thermal) density anomaly (McNutt 1988).

Typically these predicted admittances are used to filter the gravity and topography signals to determine the effectiveness of the model in reproducing the data in both the spatial and spectral domains (McNutt and Shore 1986; Fischer *et al.* 1986; McNutt 1988; Filmer and McNutt 1988; Sheehan and McNutt 1989). The ability to isolate the contribution of both the top loading due to volcanoes and the bottom loading due to a deep anomaly is a powerful tool to constrain the models. This approach is untenable for the data presented here due to both the low resolution and presence of small phase shifts. Since the data is analyzed at spacecraft altitude, the topographic signature of the volcanoes is very subtle, although still discernible in the spectral domain (see below). While less robust, this technique can still be gainfully employed by making reasonable assumptions about the scales of top (volcano) and bottom (swell) loading.

There are several caveats regarding the interpretation of admittance spectra worth noting (Forsyth 1985). If the admittance is calculated over regions of geologic processes with different gravity-topography response. functions, estimates of flexural rigid it y are biased towards those regions with the most power in the gravity and topography. In regions where both top and bottom loading are important, it is possible to mistake bottom loading for top loading if the elastic lithosphere is thin, which gives an underestimate of Te. If the elastic plate is strong, the surface load will have a larger impact on the topographic signature than the subsurface load, thus weighting the response toward top loading. For these reasons, estimates

of the effective elastic thickness determined by modeling the admittance spectra are likely t obe lower bounds.

Modeling the coherence provides a more robust estimate of effective elastic thickness since it is relative] y i nsensitive to the effects of top and bottom loading, as well as to errors in the depth of subsurface loading (Forsyth 1985). Assuming that the top and bottom loading processes have random phase (i.e. the loads are uncorrelated), the coherence is given by

$$\gamma^2 = \frac{\langle H_t W_t + H_b W_b \rangle^2}{\langle H_t^2 + H_b^2 \rangle \langle W_t^2 + W_b^2 \rangle} \qquad (1o)$$

where W_B and W_T are the relief on the crust-mantle boundary due to bottom and top loading, respectively. If the assumption of uncorrelated loads is violated, the flexural rigidity estimate is likely to be a lower bound (Macario et *al.* 1992).

RESULTS

Vertical Gravity

Vertical gravity fields produced from local point mass inversions are shown in Figs. 6-9, along with the Magellan topography for the same region. Table I contains the inversion parameters. The broad highs in gravity and topography are generally well correlated in each region. Minor phase shifts between the peaks in topography and gravity occur in most regions. At Bell Regio, the central gravity high lies between the two major volcanic edifices (Figs. 1, 6). To the north, the gravity high occurs to the east of the topographic high (Fig. 6). Gravity highs at Atla Regio are well correlated with the three major volcanic edifices, the highs along the rift flanks, and the. broad topographic swell (Fig 7). The gravity highs are shifted approximately 10 to the north of the topographic highs. At Western Eistla Regio, the western high in the gravity is exactly centered over Sif Mons, while the eastern gravity high lies somewhat to the west of Gula Mons (Fig. 8). The topography at Beta Regio is far more complex than in the other regions, with one major volcano, a large rift dissecting the center of the topographic high, and

several regions of complex ridged terrain (Senske *et al.* 1992; Bindschadler *et al. 1992).* While not all of the topographic peaks are discernible at spacecraft altitude, the complexity of the region may contribute to the relative low degree of correlation between the gravity and topography (Fig. 9) in comparison to other likely hotspots. The very large, shift in the gravity and topography peaks, approximately 4° north-south, may also be partially a result of errors in the line-of-sight accelerations clue to the very large gravity anomaly over Beta Regio. North-south shifts in the gravity highs are particularly suspect; this effect may also be evident in the 10 shift observed at Atla Regio. North-south phase shifts are not seen at Western Eistla and Bell Regiones, where the gravity highs are smaller.

Admittance and Coherence

Bell Regio. Despite numerous volcanic and tectonic features that occur on a variety of scales at Bell Regio and a space craft altitude of up to 443 km, the admittance spectrum at Bell Regio is well determined. 'l'here is good agreement between the spherical harmonic and local inversion gravity fields at most wavelengths (Fig. 10), with the exception of a 10 mgal/km offset. Possible sources of this off set and its effect on the fit of compensation models will be discussed below. I .ocal compensation, shown for depths between 25 and 150 km (Fig. 10a), provides a very poor fit to the data as the shape of the spectra do not follow the model curves.

Flexural models provide a better fit to the admittance curve. The admittance spectra calculated from the Bouger gravity anomaly are shown (Fig. 10b) along with a flexural model for with a single compensation depth of 100 km and an elastic thickness of 90 km. The long wavelength (here greater than approximately 1000 km) portion of the spectrum controls the best fitting compensation depth, Varying the compensation depth shifts the model curves vertically, with a 10 km decrease in the compensation depth resulting in an approximately 1 mgal/km decrease in the model value at long wavelength, and a slight change at short wavelength, At shorter wavelengths, the shape of the model curve is controlled by the effective elastic thickness and the proportion of top and bottom loading. The best fitting value of effective elastic

thickness is al so strong] y affected by the compensation depth, with larger depths requiring thicker elastic plates to fit the same data, The shape of the admittance spectra from both the spherical harmonic and the local inversion gravity fields indicate that both top and bottom loading are present, with bottom loading being the dominant process (Fig. 10h). A model curve with a ratio of bottom to top loading of 2.7 fits most of the spectrum.

The hotspot compensation model provides a good fit to the data (Fig. 10c). A deep compensation depth of 125 km and an effective elastic thickness of 50 km fits most of the long wavelength data very well, with a few values falling along deeper or shallower model curves. At wave.lengths between 500 and 800 km, the effect of top loading is apparent, Model curves indicate an effective elastic thickness of approximately 25-35 km. In both the top and bottom loading curves shown here, a crustal thickness of 10 km is used, The shape of the admittance spectra at short wavelengths suggests a relatively thin crust, A thicker crust gives a model curve with a somewhat shallower slope (e.g. Fig. 10c, below).

At Bell Regio, the shape of the admittance curve at short wavelength suggests that the crust is thin (-10 km), but much shorter wavelength data is necessary to obtain a reliable estimate. The vertical position and curvature of admittance spectrum together constrain the compensation depth and the effective elastic thickness. There is not enough information to independently constrain both crustal thickness and deep compensation depth used in the hotspot model. As an example of sensitivity of other parameters to the choice of crustal thickness, the hotspot model is shown with a crustal thickness of 50 km (Fig. 10c). At long wavelengths, the best fitting deep compensation depth is now 185 km rather than 125 km, but the effective elastic thickness is unchanged, Thus using a crustal thickness of 10 km probably gives a lower bound on the deep depth of compensation,

In other regions, we assume a crustal thickness value of 30 km. If the possible range of crustal thickness on Venus is between 10 and 50 km (see Discussion below), this gives an error bar of ±30 km :for the deep compensation depth. 'l'he additional 10 mgal/km uncertainty in the vertical position of the admittance spectra make the total en-or bars closer to ±35 km. Since

estimates of the deep compensation deeps arc large, the effective elastic thickness at the scale of the swell is essentially unaffected by the uncertainty in crustal thickness, However, a change in the crustal thickness has a greater effect on the estimate of elastic thickness from top loading. Although the model with a 50 km thick crust does not fit much of the short wavelength data (Fig. led), it is clear that the estimate is less (~15 km) than for the thinner crust model (Fig. 10C).

Bell Regio is the one region with an estimate of effective elastic thickness from the coherence data. Coherence estimates obtained from local inversions and spherical harmonic models typically begin to diverge at wavelengths shorter than approximately 1000 km (Fig. 10e). At high harmonics energy from features beyond the resolution of the 60 degree and order spherical harmonic model may leak into the highest order terms, causing them to be less reliable. Since the local inverse method is more suited to modeling short wavelength anomalies, we interpret the coherence estimates based on the local inversion. A model with an effective elastic thickness of 52 km and bottom to top loading ratio of. 1 fits the shorter wavelength values very well (Fig. 10e). A higher bottom to top loading ratio gives too steep a slope.

The longer wavelength values of the coherence are unusual in that they fall off below a value of 1. It is possible that this fall off indicates that surface and subsurface loads are correlated, Coherence estimates made with large box sizes in this region, using spherical harmonic data, have values closer to 1 at these wavelengths. Analyzing larger regions probably includes a wider range of processes, thus increasing the chances that loads are uncorrelated. The estimate of effective elastic thickness obtained from the coherence agrees very well with the value of the long wavelength of effective elastic thickness obtained from applying the hotspot model to the admittance. It makes sense that the coherence agrees with the regional effective elastic thickness value, since admittance tends to weight the terms with the most power. At Bell Regio, the topographic peaks are the volcanoes, which appear to have a thinner effective elastic plate.

Atla Regio. The overall shape of the admittance spectrum of Atla Regio resembles that of Bell Regio. The shape of admittance curves from the local inversion and spherical harmonic models are in very close agreement, but 10 mgal/km was again added to the spectra from the local inversion to bring the two admittance curves into agreement. As seen in Fig. 11a, isostatic compensation does not fit the data well. The addition of the effects of lithospheric flexure are clearly needed to provide a good fit to the data (Fig. 11 b). A model curves with an effective elastic thickness of 100 km, a compensation depth of 150 km and predominantly hot tom loading fits the long wavelength portion of the spectrum very neatly. Between 400 and 500 km, a model with a ratio of bottom-to-top loading of 5 fits the data, but data at medium wavelengths can not be fit the same model, A thinner effective elastic thickness loaded from below could fit just the data between S00 and 800 km.

The hotspot model also gives a reasonable fit to the data at Atla Regio (Fig. 11c). Assuming a crustal thickness of 30 km, a model with a swell compensation depth of approximately 175 km and an effective elastic thickness of 30 ± 5 km fits much of the. data down to a wavelength of S00 km. A top loading signature appears between 400 and 500 km and indicates an effective elastic thickness of 30±10 km.

The coherence data at Atla Regio have a much shallower slope than the model curves (Fig. 11 id), indicating that a model with uncorrelated loads and a single elastic thickness is not applicable in this area, and that the coherence can not provide an estimate of effective elastic thickness.

Western Eistla Regio. Despite the relat ive simplicity of the large scale tectonics of Western Eistla Regio, there is much more scatter in the. admittance spectra than at Atla and Bell Regiones, which results in less agreement between the spectra for local and global models gravity models (Fig. 12). The large value of the line-of-sight angle, 80°, maybe responsible for the poor quality of the data, The fit of the data to the three compensation models is shown for consistency, but errors in the data mean that the compensation mechanism and effective elastic thickness can only be constrained in a qualitative manner. As with other regions, Airy

compensation does not give a good fit to data (Fig. 12a). Within the scatter in the data, the addition of flexure provides a better fit (Fig. 12b). A model with an elastic thickness of 130 km, a compensation depth of 200 km, and a ratio of bottom-to-top loading of 4 comes close to fitting a significant portion of the spectra,

The hotspot model of compensation also generally follows the shape of the admittance curve (Fig. 12c). The upturn in the spectra between 500 and 800 km are characteristic of top loading, but the difference between the local inversion and spherical harmonic models combined with the scatter in the data make this signature suspect, An effective elastic thickness of 40±10 km fits most of the data, A fairly large range of deep compensation depths and effective elastic thicknesses can fit the long wavelength data. Fig. 12c shows the fit to the data for a models with a 30 km thick crust, an effective elastic thickness of 40 km, and compensation depths between 125 and 225 km,

There is a lot of scatter in the coherence spectrum of Western Eistla Regio (Fig. 12d). Effects such a coherent loading and variations in the effective elastic thickness can cause scatter in the coherence data (Forsyth 1985). It is interesting, although probably not significant, that the coherence seems to have two branches that follow model curves for effective elastic thicknesses of approximately 60 and 90 km. Careful forward modeling would be required to verify the possibility that two distinct effective elastic thicknesses could be resolved in the coherence.

Beta Regio. The scatter in the admittance and coherence at Beta Regio is sufficiently large to make any interpretation of compensation mechanism difficult. The line-of-sight angle is large at Beta Regio, 65°. It is less than the value of 72° at Atla Regio, but the lower spacecraft altitude at Atla Regio may counteract the poor observing geometry. The data quality at Beta Regio may also be influenced by the very large, long wavelength high in the gravity that could cause ringing in the solution. The local inversion is more sensitive to this problem than the spherical harmonic model, as longer data arcs are used with the global fit. As with the other regions, isostatic compensation models do not adequately describe the spectra (Fig. 13a). Models that

include flexural compensation fit portions of the admittance curve (Fig. 13b). The upswing in the Bouger admittance at short wavelengths suggests bottom loading is important, but no single loading model fits the data. The fit of the hotspot model to the free air admittance similarly suggests that bottom loading is important, but the scatter and large error bars prohibit a well determined estimate of either compensation depth or effective elastic thickness (Fig. 13c). An effective elastic thickness of 40 km with a swell compensation depth of 200-300 km fits a significant portion of the data, Unlike the other three regions, there is no evidence for a top loading signature, despite the presence of Thea Mons. The effect of Thea Mons on the gravity and topography may be relatively minor at Beta Regio, given the complexity of the geology and topography, in comparison to other areas where volcanoes are a more dominant part of the topography. Alternatively, the data quality may be too low to recognize the top loading signature. If the elastic lithosphere under Thea Mons is 20 km or less, the resolution of the data is insufficient to recognize a contribution. As with Atla Regio, the slope of the coherence is very shallow (Fig. 13d). Given the variety of tectonic and volcanic features at Beta Regio, it is more likely that the low slope is a result of multiple elastic thicknesses than the presence of correlated loads,

The Flexural model vs. the Hotspot Model

A purely isostatic model can clearly be ruled out for Bell and Atla Regiones. For Atla and Bell Regiones, it is not possible to distinguish between the flexural model, which includes bottom and top loading with a single elastic thickness and compensation depth, and the hotspot model, which has top loading, crustal compensation and a given elastic thickness at short wavelengths, and bottom loading, crustal compensation, an effective elastic thickness (possibly different from that at short wavelength) and an additional, deep compensation surface. Both models fit the data reasonably well. The flexural models yield very high values of effective elastic thickness (approximately 100 km) the model has only one compensation depth. The fit to the long wavelength portion of the spectra gives compensation depths in the range of 100-

200 km. These large values of compensation depth require very large values of effective elastic thickness to match the curvature of the spectra. 'lie hotspot model yields effective elastic thickness estimates of 20-50 km because it includes both compensation at the crust mantle boundary and at a deep surface, presumably the base of the thermal lithosphere.

We believe that the simple flexural model can be rejected for a variety of reasons. The first set of arguments hinges on discounting the estimates of approximately 100 km for the effective elastic thickness. On the basis of this study, this value disagrees with the one robust estimate of effective elastic thickness obtained using coherence, which is less sensitive to uncertainties in the other model parameters. At Bell Regio, the coherence yields an effective elastic thickness equal to 52 km, in very good agreement with the estimate of the long wavelength flexural thickness obtained from the hotspot model. Effective elastic thicknesses of 20-50 km are also in very good agreement with estimates from other studies that are based on the analysis of topographic data in a variety of geologic settings (Solomon and Head 1990; Sand well and Schubert 1992; Johnson and Sandwell 1994). The value of 30±1 O km for the short wavelength, top-loaded effective elastic thickness at Bell Regio is also in good agreement with the estimate of 10-20 km made by McGovern and Solomon (1992) from a flexural moat at Tepev Mons. This estimate has an error of approximately*15 km (McGovern, personal communication, 1993).

Other arguments are based on the assertion that the hotspot model is more appropriate for these areas than the simple flexural model, Compensation depths obtained from the flexural model arc far to large to be related to a density contrast at the crust-mantle boundary. The presence of a crustal layer on Venus is widel y accepted, with the strongest evidence coming from Soviet Venera lander measurements of the isotropic signature of the surface (Barsukov *et al. 1984).* Other studies of the mechanical properties of tectonic features indicate that the thickness of the crust is between 10 and 30 km (Zuber 1987; Grimm and Solomon 1988; Banerdt and Golombek 1988; Zuber and Parmentier 1990). However, a new flow law for dry diabase (Mackwell *et al.* 1993) may indicate that the crust is stronger on Venus than previous] y

believed, which would tend to make previous estimates of crustal thickness lower bounds. It is reasonable to assume that the crust in these areas contributes to the compensation. Lastly, the commonalities between the regions studied here and terrestrial hotspots are a further indication that the hotspot model is the most appropriate model to apply in this tectonic setting. For example, it is cleat that volcanoes with diameters on the order of a hundred kilometers load the elastic plate from above. This information should be incorporated into the model.

The poor data quality at Beta and Western Eistla Regiones do not permit detailed interpretations. However, the general shape of the admittance spectra is more consistent with a flexural response than with purely local compensation, Neither the flexural model nor the hotspot model give well constrained values of effective elastic thickness. However, the values of effective elastic thickness found at Beta and Western Eistla Regiones, 40±20 and 40±30 km, respective] y, using the hotspot model, and 100 km in both regions using the flexural model, are comparable to the better determined values found at Bell and Atla Regiones.

Comparison to Previous Studies.

Previous studies of Pioneer Venus gravity and topography data resolved primarily wavelengths greater than approximately 500-1000 km and were unable to determine the effective elastic thickness. Numerous studies found compensation depths for some or all of the four hotspots considered in this study (Esposito et *al.* 1982; Sjogren *et al.* 1984; Janale *et al. 1987;* Herrick *et* al. 1989; Smrekar and Phillips 1991; Black *et al.. 1991;* Grimm and Phillips 1992). Within the range of uncertainty and variations in methodology, results from this study are generally in agreement with earlier work.

Comparison to Terrestrial Hotspots.

As noted in previous studies, the apparent long wavelength depth of compensation is much greater than for terrestrial oceanic hotspots, probably due to the decoupling effect of the terrestrial low viscosity zone (Smrekar and Phillips 1991, Kiefer and Hager 1991). It is

interesting to note that while the deep structure appears to be quite different, the effective elastic thicknesses determined in this study are very similar to values obtained for both oceanic and continental hotspots (McNutt and Shore 1986; Fischer *et* al. 1986; McNutt 1988; Sheehan and McNutt 1989; Ebinger *et al.* 1989). The admittance spectra found at Bell Regio is similar in shape to that of the Burmuda Rise, where the elastic lithosphere at short wavelength is 30±5 km and 55±1O km at long wavelength (Sheehan and McNutt 1989). However at the Burmuda Rise, the swell compensation depth is 55 km, and the difference in effective elastic thickness is interpreted as a result of thermal thinning.

DISCUSSION

The Case for Active Hotspots.

At Atla Regio, the very large depth of swell compensation and the clear signature of bottom loading are strong evidence of a significant thermal anomaly at depth. Studies of the emissivity at Maat Mons (Robinson and Wood 1993) and of the removal of impact crater halos in Atla Regio (Basilevsky 1993) appear to support the conclusion that Atla Regio is an active, or recently active, hotspot. Bell Regio has a much shallower compensation depth and a large effective elastic thickness. As is discussed below, these results may indicate that Bell Regio is inactive. At Beta and Western Eistla Regiones, only the deep, long wavelength depth of compensation suggest an active hotspot. The validity of the argument that large compensation depths, even without a bottom loading signature, imply the presence of an active hotspot is discussed next.

In several previous studies (Phillips *et al.* 1981; Morgan and Phillips 1983; Phillips and Malin 1983,1 984; Herrick *et al.* 1989; Srnrekar and Phillips 1991), these regions were interpreted as active hotspots because their long wavelength compensation depths are greater than the depth to the inferred base of the thermal lithosphere. A compensation depth greater than the thickness of the thermal lithosphere was interpreted to indicate that an active plume was

supplying a viscous stress at depth that was helping compensate the hotspots. Estimates of the thickness of the thermal lithosphere were based on the idea that the heat loss and level of tectonic activity on Venus is comparable to Earth's (Solomon and Head 1982; Kaula and Phillips 1981; Phillips and Malin 1983).

These assumptions about the thickness of the thermal lithosphere have been reevaluated in light of studies of both impact crater distribution and effective elastic thickness. One interpretation of the large crater retension age is that tectonic activity on Venus is episodic, and that the lithosphere has been steadily cooling and thickening over the last 500 My (Tucotte 1993), reaching thicknesses of 200-300 km. In the context of this hypothesis, the large compensation depths at hotspots would indicate thinning of the thermal lithosphere. However, Beta and Atla Regiones have among the highest geoid/topography admittance values, or, equivalently, compensation depths, on the planet (Simons et al. 1994). Thus the background thickness of the thermal lithosphere must be less than the compensation depth at Beta and Atla Regiones. Evidence from interpretation of long wavelength gravity still supports a thermal lithospheric thickness of approximately 100 km.

The argument that very large compensation depths, greater than approximately 100 km, implies active mantle plumes is still generally valid. The challenge is to understand how active hotspots fit into the resurfacing puzzle. Probably the simplest interpretation is that they represent a localized contribution to resurfacing. Resurfacing on scales less than the intracrater distance of approximately 400 km is consistent with the cratering record (Phillips *et al.* 1992). Although the broad swell covers a large area, the volcanism clearly related to the swell formation (i.e. the shield volcanoes and associated flows) covers a much more limited region. At Beta Regio, large areas of tessera terrain, that are believed to be remnants of a prior tectonic period (Senke et al. 1992), occur high on the swell but are largely untouched by volcanism. More minor tessera blocks also occur at Bell Regio. The substantial area of rifts at Atla Regio are largely devoid of volcanism (Solomon et al. 1992). Large expanses of ridged plains appear to be uplifted at Western Eistla Regio (Grimm and Phillips 1992; Stofan *et al.* 1994).

New information about the rheology of very dry diabase (Mackwell *et al.* 1993) indicate that large estimates of effective elastic thickness (-30 km) are not at odds with a reasonable thermal gradients on Venus, The lack of water on Venus appears to compensate for the high temperature, giving a rheology more similar to Earth than previously believed, Thus for modest stresses and thermal gradients, the upper few tens of kilometers of the crust will respond elastically (Phillips 1994).

Implications for Hotspot Evolution

In the context of simple models of hotspot evolution (Olsen and Nam 1986; Griffiths *et al.* 1989; Griffiths and Campbell 199 l; Smrekar and Parmentier 1994), regions with very large compensation depths, such as Beta, Atla, and probably Western Eistla Regiones, are in an early to intermediate stage of evolution. Each of this regions has large compensation depths, abundant volcanism, and evidence for extension. Geologic and morphology evidence supports this hypothesis (Stofan *et al. 1994).*

The variations in compensation depth alone between Beta, Atla and Western Eistla Regiones probably can not be related to evolutionary stage. For example, it is unlikely that Beta Regio is younger than the other areas simply because it has a somewhat larger compensation depth. The abundance of volcanism at Beta Regio suggests that it is not in a very early stage of evolution where the plume has not fully flattened out and thus gives a large compensation depth. Variations in compensation depth are more likely to be a result of local variation in either the plume strength or the lithosphere.

Bell Regio differs from the other area in several ways. The relatively shallow compensation depth, the large value of long wavelength effective elastic thickness, and the small bottom-to-loading ratio determined from the coherence all imply that Bell Regio is in a late stage of evolution, possibly even extinct. The small bottom loading may be due to either the remnant of a thermal anomaly or possibly the effect of a layer of low density residuum material implaced at the depth as result of pressure release melting (Robinson 1988). Such an effect is likely to be

much more important on Venus than on Earth because of the absence of plate tectonics. Hotspots are not carried to a new location by plate motion, so that the residuum layer can continue to accumulate. The lack of subduction may mean that residuum material is not recycled as rapidly into the mantle (Parmentier and Hess 1993). Geologic evidence also suggests that Bell Regio is in a late stage of evolution (Stofan et al. 1994).

The hotspot model gives a long wavelength effective elastic thickness of 50±5 km, and a short wavelength, top loading effective elastic thickness of 30±10 km. This difference may be due to an underestimate of the short wavelength value of effective elastic thickness by a purely top loading model. If the difference is real, thereat least two interpretations. One is that the elastic lithosphere under the volcanoes is thermally thinned, This interpretation appears to be at odds with the coherence modeling, which gives a ratio of bottom-to-top loading is approximately 0.1. If a thermal anomaly large enough to cause approximately 30 km of thermal thinning were present under Bell Regio, bottom loading should be much more important.

Another interpretation is that the two values sample different points in the time evolution of a hotspot. Early on, the increase in heat flow due to a mantle plume hitting the base of the lithosphere can cause thinning of the thermal and elastic lithosphere (e.g. Sheehan and McNutt 1989). As the mantle plume dies out, the elastic thickness will again increase and the bottom loading will decrease as the thermal anomaly dies out. The value of approximately 30 km may reflect the thickness of a thinned elastic plate that was present at the time when the plume strength was at a maximum and the volcanoes were implaced. Since the load of the volcano does not change after it is implaced and features with a diameter of several hundred kilometers can be fully supported by an elastic thickness of 30 km, the topography would not readjust to an increase in the thickness of the plate. However, the long wavelength topographic swell, which is only supported by the elastic plate to a very small degree, will continue to adjust to changes both in the elastic thickness and in the decreasing bottom load and would thus give a more accurate indication of present-day conditions. The value of effective elastic thickness

obtained is likely to be somewhat biased by the response of both the growing elastic plate and the changing bottom load, perhaps towards a lower value.

Several workers have suggested that hotspot evolution follows a somewhat different path on Venus than on Earth. If the crust is very weak on Venus, especially in an area of high heat flow, the crust above a hotspot might become very thin, resulting in a topographic low over hotspots (Bindschadler and Parmentier 1990; Grimm and Phillips 1990). Herrick and Phillips (1990) proposed an evolutionary sequence in which hotspots evolve into crustal plateaus due to the production of large volumes of pressure release melting. New estimates of effective elastic thickness indicate that the crust is quite strong, even over active hotspots. Thus crustal thinning over hotspots is likely to be less important than previously suggested. It is more difficult to access the hypothesis that large volumes of crust are generated at hotspots. Bell Regio appears to have entered a late stage of evolution without having produced a crustal plateau. I lowever, Bell Regio is among the smaller hotspots and possible hotspots, and it may represent a less vigorous mantle upwelling.

Further Work.

This study represents a first look at the data available to date over four of Venus' major volcanic swells, or hotspots. Clearly Magellan gravity data represent a vast improvement in quality and resolution over Pioneer Venus gravity data. Data that is currently being collected by Magellan, now in a nearly circularized orbit, is likely to represent an additional increase in data quality in some regions, particularly at high latitudes and in areas where the viewing geometry is improved, These data may make it possible to better constrain the compensation mechanisms at Beta and Western Eistla Regiones and to determine more accurate estimates of effective elastic thickness. Smaller regions, such as Imdr and Dione Regiones, that are also canidates for hotspots will be covered at relatively low altitudes. Improved data analysis and further modeling of the gravity data should eliminate phase shifts and permit better spatial analysis. Better coherence estimates would be extremely useful for determining very robust estimates of

flexural thickness and the relative magnitude of surface and subsurface loads. Another important step is more localized studies of somewhat smaller regions. For example, it would be very informative to try to isolate the signature of the rifts at Atla Regio. Forward models of specific processes, such as thinning of the elastic plate, might also offer some additional insight. Differences in the base level for spectra calculated using local inversions and spherical harmonic models of the gravity must be resolved.

CONCLUS1ONS

"J-he spectral admittance calculated from the topography and gravity data, from both local inversions and spherical harmonic models, for Atla, Beta, Bell, and Western Eistla Regiones have been compared with three models of compensat ion: local, local and surface and subsurface loading (Forsyth 1985), and a hotspot model (McNutt and Shure 1986) that includes top loading (by volcanic edifices) at short wavelengths, and bottom loading at long wavelength due a deep (presumably thermal) density anomaly. In all models, the longest wavelengths, greater than approximately 1200 km, are unaffected by flexure. The long wavelength, apparent depths of compensation for Bell, Atla, Western Eistla, and Beta Regiones are 125, 175, 200, and 250 km, respectively, in good agreement with previous studies. The uncertainty on these values is no more than ±35 km.

Spectra for Atla and Bell Regiones exhibit a clear signature of both bottom and top loading of the elastic plate, thus ruling out a purely local compensation mechanism. Data quality at Beta and Western Eistla Regiones is relatively poor. Isostatic compensation can not be conclusively ruled out, but the shape of the spectra are consistent with bottom loading at Beta Regio and top and bottom loading at Western Eistla Regio. Both the flexural model and the hotspot model fit the data at Atla and Bell Regiones very well. Neither model can be eliminated on the basis of fit to the data alone. However, we believe the flexural model can be ruled on other grounds. The estimates of effective elastic thickness obtained from the fit of the flexural model to the data are

all approximately 100 km, This value is much larger than estimates obtained from analysis of the topography in other regions of Venus (Solomon and I-1ead 1990; Sand well and Schubert 1992; Johnson and Sandwell 19994), and at Bell Regio (McGovern and Solomon 1992). In this study, we obtain a robust estimate of 52 km for the effective elastic thickness from the coherence spectra at Bell Regio. This value is in excellent agreement with the long wavelength estimate obtained with the hotspot model, Further, the hotspot model is more appropriate for these regions. The large volcanic edifices found at each of the highlands clearly load the surface at short (several hundred kilometer) wavelengths. The hotspot model includes both crustal and deep compensation surfaces. Deep compensation is obvious in these areas and crustal compensation is likely.

The hotspot compensation model results illustrate important differences in the four hotspots. At Atla Regio, the model fit gives an effective elastic thickness of 30 km and a deep compensation depth of 175 km, assuming a crustal thickness of 30 km. The data indicate both a top loading signature at short wavelength and bottom loading signature at long wavelength. Both the compensation depth, which larger than is typical of the rest of the planet, and the bottom loading signature are indicative of an active hotspot. The quality of the data at Beta and Western Eistla Regiones do not allow a detailed interpretation of the compensation mechanisms. However, the large compensation depth of 150 km or more at Western Eistla Regio and a depth of 250 km at Beta Regio support the interpretation that these areas are underlain by large thermal anomalies probably due to active mantle plumes.

The signature at Bell Regio is clearly different from the other regions. The fit to the coherence data confirm that the long wavelength effective elastic thickness is 52 km, with a bottom-to-top loading ratio of 0.1, The relatively shallow depth of compensation (125 km), the large effective elastic thickness, and small bottom load all indicate that Bell Regio is in a very late, possibly inactive, evolutionary stage. The small magnitude of bottom loading maybe consistent with loading by a low density layer of residuum due to melt extraction, suggesting that there may no longer be a thermal anomaly underneath Bell Regio. The fit of the model to

the admittance spectrum indicates that the effective elastic thickness is smaller, approximately 30±5 km, at short wavelengths than at larger scales, closer to the dimension of the swell, where the effective elastic thickness is 50±5 km. This difference may be a result of fitting a top loading model only to the short wavelength data. If the difference is real, the small elastic plate thickness estimate may be preserved from an earlier time of higher heat flow when the volcanoes were implaced, while the thicker value represents the present-da y state. A small value of bottom loading is inconsistent with present-day thermal thinning of the elastic lithosphere from 50 to 30 km underneath the volcanoes.

These early results from a survey of the four major volcanic swells on Venus reveal hotspots in different stages of evolution. Analysis confirms that Beta, Atla and Western Eistla Regiones are active hotspots. The variation in compensation depths between these three areas probably indicate variations in the strength of the plume or differences in the lithospheric structure rather than different stages of evolution, Bell Regio appears to be in a very late stage of evolution, possibly inactive. Estimates of the effective elastic thickness show that the near surface layer is much stronger than previously believed, suggesting that little crustal thinning due to ductile flow occurs over hotspots. Future studies of other possible hotspot on Venus and analysis of new data for these regions, along with studies of their geologic history (Stofan *et al.* 1994) will continue to improve our understanding of hotspot evolution on Venus and Earth.

ACKNOWLEDGEMENTS

1 am grateful for the assistance of George Hu, who ran several of the local inversions presented here. This paper was improved through conversations with Roger Phillips, who also supplied local portions of the spherical harmonic gravity and topography fields. This work has been supported by the Venus Data Analysis Program, NASA grant 889-62-02.

REFERENCES

Banerdt, W. B., and M. P. Golombek (1988), Deformational models of rifting and folding on Venus, *J. Geophys. Res.* 93, 4'759-4772.

Barsukov, V. IL., Yu. A. Surkov, L. P. Moscalyeva, V. P. Kharyukova, and A. L. Kemurdzjan (1984). Studies of the composition, texture and properties of the rocks on Venus by Venera 13 and Venera 14, Proc. Lunar Planet. Sci. Conf. 14th, in *J. Geophys. Res.* 89, 393-402.

Basilevsky, A. T, (1993). Age of rifting and associated volcanism in Atla Regio, Venus, *Geophys. Res. Lett.* 20, 883-886.

Bendat, J. S., and A, G. Piorsol (1980). *Engineering Applications of Correlation and Spectral Analysis, p. 274,* John Wiley, New York.

Bercovici, D., G. Schubert, and G. A, Glatzmaier (1989). Influence o fheating mode on three-dimensional mantle convection, *Geophys. Res. Lett.* 16,617-620.

Bindschadler, ID. L., and E. M.Parmentier(1990). Mantle flow tectonics: Ther influence of a ductile lower crust and implications for the formation of topographic uplands on Venus. *J. Geophys. Res.* 9S, 21,329-21,344.

Binschadler, D. L., G. Schubert, and W. M. Kaula (1992). Coldspots and hotspots: Global tectonics and mantle dynamics of Venus. *J, Geophys. Res.* 97, 13,495-13,532.

Black, M. 'l'., M, 'I'. Zuber, and D. C. McAdoo (1991), Comparison of observed and predicted gravity profiles over Aphrodite Terra, Venus, *J. Geophys. Res.* 96, 301-315.

Campbell, D. B., J. W. Head, J. K. Harmon, and A. A. Hine (1984). Venus: Volcanism and rift formation in Beta Regio. Science 226, 167-170.

Davies, G.F. (1988). Ocean bathymetry and mantle convection 1. Large-scale flow and hot spots, *J. Geophys. Res.* 89, 10,467-10,480.

Davies, G. F. (1992). Temporal variation of the Hawaiian plume flux. *Earth Planet. Sci. Lett.* **113,** 277-286.

Ebinger, C. J., T, D. Bechtel, D. W. Forsyth, and C. O. Bowin (1989). Effective elastic plate thickness beneath the East African and Afar plateaus and dynamic compensation of the uplifts, *J. Geophys. Res.* 94, 2883-2901,

Esposito, P. B., W. L. Sjogren, N. A. Mottinger, B. G. Bills, E. Abbott (1982). Venus gravity: Analysis of Beta Regio, *Icarus* **51**, 448-459.

Filmer, P, E., and M. K, McNutt (1989). *Marine Geophy. Res.* 11,770-87.

Fischer, K., McNutt, M. K., and L. Shure (1986). Thermal and mechanical constraints on the lithosphere beneath the Marquesas swell, *Nature, 322,733-736.*

Ford, P. G., and G. H. Pettengill (1992). Venus topography and kilometer-scale slopes. *J. Geophys.* Res. 97, 13,103-13,114.

Forsyth, D. W. (1985). Subsurface loading and estimates of the flexural rigidity of the continental lithosphere. *J. Geophys. Res.* 90, 12,623-12,632.

Grimm, R. E., and S. C. Solomon (1988). Viscous relaxation of impact crater relief on Venus: Constraints on crustal thickness and thermal gradient. *J. Geophys. Res.* 93, 11,911-111,929.

Grimm, R.E., and R.J. Phillips (1988). Gravity anomalies, compensation mechanisms, and the geodynamics of western Ishtar Terra, Venus. *J. Geophys. Res.* 93, 11,911-11,929.

Grimm, R. E., and R.J. Phillips ()992). Anatomy of a venusian hot spot: geology, gravity and mantle dynamics of Eistla Regio. *J. Geophys. Res* 97, 16,035-16,054.

Griffiths, R.W., and I.H. Campbell (1991). Interaction of mantle plume heads with the Earth's surface and onset of small-scale convection. *J. Geophys. Res.* 96, 18,295-18,310.

Griffiths, R.W., M. Gurnis, and G. Eitelberg (1989). Holographic measurements of surface topography in laboratory models of surface hotspots. *Geophys. J.* 96, 477-495.

Herrick, R. R., B. G. Bills, and S. A. Hall (1989). Variations in effective compensation depth across Aphrodite Terra, Venus. *Geophys. Res. Lett.* 17, 1337-1340.

Herrick, R. R., and R. J. Phillips (1 990). Blob tectonics: A prediction for western Aphrodite Terra, Venus. *Geophys. Res. Lett.* **17**, *2129-2132.*

Janale, P., D. Jannsen, and A. T. Basilevsky (19$7). Morphologic and gravimetric investigations of Bell and Eisila Regiones on Venus. *Earth Moon Planets 39,251-273.*

Johnson, C. L., and D. T. Sandwell (1994). Lithospheric flexure on Venus. *J. Geophys. Res. submitted.*

Kiefer, W. S., and B. H. Hager (1991). A mantle plume model for the equitoial highlands of Venus. *J. Geophys. Res.* 91, 401-419.

Konopliv, A. S. and W. 1.. Sjogren (1994). Venus spherical harmonic gravity model to degree and order 60, *Icarus, this issue.*

Macario, A., A. Malinverno, and W.F. Haxby (1992). On the robustness of elastic thickness estimates obtained using coherence methodology: Application to the Alps. *Eos Trans. Am. Geophy. Un. 73, 571.*

Mackwell, S. ,1., D. L. Kohlstedt, D. S. Scherber, and M. E. Zimmerman (1993). High temperature deformation of diabase: implications for tectonics on Venus (abs). *Eos, Trans. Am. Geophys. Un., Fall Meeting 74, 378.*

Manga, M., H. A. Stone, and R. J. O'Connell (1993). The interaction of plume heads with compositional discontinuities in the Earth's mantle. *J. Geophys. Res.* 98, 19,979-19,990.

McGill, G. E., S. J. Steen strup, C. Barton, and P. G. Ford (1981). Continental rifting and the origin of Beta Regio, Venus. *Geophys. Res. Lett.* **8,** 737-740.

McGovern, P. J., and S. C. Solomon (1992). Estimates of elastic plate thickness bcbeath large volcanos on Venus (abs). *Int. Co/l. on Venus,* p. 68, Lunar Planet. Inst.

McKenzie, D., and C. Bowin (1976). The relationship between bathymetry and gravity in the Atlantic. Ocean. *J. Geophys. Res. 81, 1903-1915.*

McNutt, M. (1979). Compensation of oceanic topography: An application of the response function technique to the *Surveyor* Area. *J. Geophys. Res 84,7589-7598.*

McNutt, M.K. (1983). Influence of plate subduction on isostatic compensation in northern California. *Tectonics 2, 399-415.*

McNutt, M. (1988). Thermal and mechanical properties of the Cape Verde Rise. *J. Geophys. Res.* 93, 2784-2794.

McNutt, M,K., and K.M. Fischer (1 987). The south Pacific superswell. In *Seamounts, Islands, and Atolls (B.* H. Keating, P. Fryer, R. Batiza, G, W. Boehlert, Eds.), pp. 25-34. Am. Geophys. Un., Washington.

McNutt, M., and L.. Shure (1986). Estimating the compensation depth of the Hawaiian swell with linear filters. *J. Geophys. Res.* **91,** 13,915-13,923.

Menke, W. (1984). *Geophysical Data Analysis: Discrete inverse Theory.* Academic Press, Austin,

Moresi, L., and B. Parsons (1994). Interpretating gravity, geoid and topography for convection with temperature dependent viscosity: Application to surface features on Venus. *J. Geophys. Res. submitted.*

Morgan, P. and R. J. Phillips (1983). Hot spot heat transfer: Its application to Venus anti implications to Venus and Earth. *J. Geophys. Res.* **88,** 8305-8317.

Munk, W.H., and D.E. CartWright (1966). Tidal spectroscopy and prediction. *Philos. Trans. R. Sot. London, Ser. A,* **259,** *533-589.*

Olson, P., and 1. S. Nam (1986). Formation of seafloor swells by mantle plumes. *J. Geophys. Res.* 91, 7181 -7 191.

Parmentier, E. M., and P. C. I less (1992.). Chemical differentiation of a convecting planetary interior: Consequences for a one plate planet such as Venus, *Geophys. Res. Lett.* **19,** 2015-2018.

Pettengill, G. H., P. G. Ford, W. T. K. Johnson, R. K. Raney, and L. A. Soderblom (1991). Magellan: Radar performance and data products, *Science 252,260-265.*

Phillips, R. J., W. L. Sjogren, and E. A. Abbott (1978). Simulation gravity modeling to spacecraft-tracking data: Anal ysis and application. *J. Geophys. Res.* **83,** 1978.

Phillips, R. J. (1994). Evaluation of venusian highland models. *Icarus, this issue.*

Phillips, R. J., W. M. Kaula, G. E. McGill, and M. C. Malin (1981). Tectonics and evolution of Venus. *Science 212, 879-887.*

Phillips, R. J. and M, C. Malin (1983), The interior of Venus and tectonic implications, in *Venus, eds.* D. M. Hunten, L. Colin, T. M. Donahue, and V. I. Moroz, Univ. Arizona Press, Tucson.

Phillips, R. J. and M. C. Malin (1984). Tectonics of Venus, *Ann. Rev. Earth P/ant/. Sci. 12, 411-443.*

Phillips, R. J., R, E. Grimm, and M. C. Malin (1991), Hot spot evolution of the global tectonics of Venus, *Sci.* 252, 651-658.

Phillips, R. J., R.R. Herrick, R.E. Grimm, R.F. Raubertas, J.C. Sarkar, R.E. Arvidson, and N. Izenberg (1 992). Impact crater distribution on Venus: implications for planetary resurfacing, *J. Geophys. Res.* 9715,923-15,948.

Robinson, C. A., and J. A. Wood (1993). Recent volcanic activity on Venus: Evidence from radiothermal emissivity measurements. *Icarus* **102**, *26-39.*

Robinson, E. M. (1988). The topographic and gravitational expression of density anomalies due to melt extraction in the uppermost oceanic mantle. *Earth Planer. Sci. Lett. 90,221-228.*

Sandwell, D. T., and K.R. MacKenzie (1989). Geoid height versus topography for oceanic plateaus and swells. *J. Geophys. Res.* 94, 7403-7418.

Sandwell, D. T. and G. Schubert (1992). Flexural ridges, trenches, and outer rises around coronae on Venus. *J. Geophys. Res.* 97, 16,069-16,084.

Schaber, G. G. (1982). Limited extension and volcanism along zones of lithospheric weakness. *Geophys. Res. Lett.* **9**, *499-502.*

Schaber, G. G., R.G. Strom, H.J. Moore, L.A. Soderblom, R.L. Kirk, D.J. Chadwick, D. I>. Dawson, L.R. Gaddis, J.M. Boyce, and J. Russell (1992). Geology and distribution of impact craters on Venus: What are they telling us? *J. Geophys. Res.* 97, 13,257-13,302.

Senske, D. A., G.G. Schaber, and E.R. Stofan (1992). Regional topographic rises on Venus: Geology of Western Eistla Regio and Comparison to Beta Regio and Atla Regio. *J. Geophys. Res.* 97, 13,395-13,13,420.

Sheehan, A. F. and M. K. McNutt (1989). Constraints on thermal and mechanical structure of the oceanic lithosphere at the Burmuda Rise from geoid height and depth anomalies, *Earth Planet. Sci. Lett. 93, 377-391.*

Simons, M., B. H. Hager, and S. C. Solomon (1993). Regional variations in the geoid.holography admittance of Venus. Submitted to *Science.*

Sjogren, W. L., R. J. Phillips, P. W. Birkeland, and R. N. Wimberly (1980). Gravity anomalies on Venus. *J. Geophys. Res. 85, 8295-8302.*

Sjogren, W. L., B.G. Bills, P.W. Birkeland, P.B. Esposito (1983). A.R. Konopliv, N A. Mottinger, and S.J. Ritke. Venus gravity anomalies and their correlations with topography, *J. Geophys. Res.* 88, 1119-1128.

Sjogren, W. L, and R. J. Phillips (1994) The Magellan gravity experiment, *Icarus, this issue.*

Sleep, N. H., Hotspots and mantle plumes: Some phenomonology, *J. Geophys. Res., 95,* 6715-6736, 1990.

Smrekar, S.E. and E.M. Parmentier (1994). Time evolution of mantle plume-lithosphere interaction on Venus, in preparation.

Smrekar, S.E. and R.J. Phillips (1989). Implications of gravity modeling for a thermal isostasy hypothesis for Bell Regio, Venus, *Lunar Planet. Sci. 20, 1028-1029,* LPI, Houston.

Smrekar, S., and R.J. Phillips (1991). Venusian highlands: Geoid to topography ratios and their interpretation, *Earth Planet. Sci. Lett.* 107, 582-597.

Solomon, S. C. and J. W. Head (1982). Mechanisms for lithospheric heat transport on Venus: implications for tectonic style and volcanism, *J. Geophys. Res.* 87,9236-9246.

Solomon, S. C., and J. W. Head (1990). Lithospheric flexure beneath the Freyja Montes foredeep, Venus: Constraints on lithospheric thermal gradients and heat flow. *Geophy. Res. Lett.* **17**, 1393-1396.

Solomon, S. C., S.E. Smrekar, D.L. Bindschadler, R.E. Grimm, W.M. Kaula, G.E. McGill, R. J. Phillips, R.S. Saunders, G. Schubert, S.W. Squyres, and E.R. Stofan (1992). Venus tectonics: An overview of Magellan observations, *J. Geophys. Res.* 97, 13,199-13,256.

Stofan, E, R., J.W. Head, D, II, Campbell, S.H. Zisk, A.F. Bogomolov, O.N. Rzhiga, A. T. Basilevsky, and N. Armand (1989). Geology ofarift zoneon Venus: Beta Regio and Devan Chasma. *Geol. Soc. Am. Bull.* **101**, 143-156.

Stofan, E. R., D. Binschadler, D. Senske, and S. E. Smrekar (1994). Geologic and morphologic evidence for hotspot evolution on Venus. *In preparation.*

Turcotte, 1>.1.., An episodic hypothesis for Venusian tectonics (1 993). *J. Geophys. Res.* 98, 17,061-17,068.

Zuber, M. T. (1987). Constraints on the lithospheric structure of Venus from mechanical models and tectonic surface features. *J. Geophys. Res.* 92, E541-E55 1.

Zuber, M. T. and E. M. Parmentier (1990). On the relationship between isostatic elevation and the wavelength of tectonic surface features on Venus, *Icarus* 8S, 290-308.

Zuber, M.T., T.D. Bechtel, and D.W. Forsyth (1 989). Effective elastic thicknesses of the lithosphere and mechanisms of isostatic compensation in Australia. *J. Geophys. Res.* 94, 9353-9367.

Area	Atla Regio	Bell Regio	Beta Regio	Western Eistla Regio
latitude (deg)	- 10S to 25N	20 to 40N	16 to 39N	10 to 33N
longitude (deg)	180 to 215E	40 to 60E	272 to 295E	343 to 10E
# point masses	2116	1280	1156	1292.
point mass spacing (deg)	1	1	1	1
# singular values retained	306	266	386	502
# of data orbits	62	46	45	57
range of orbit numbers	6762-7005	6053-6250	7225-7403	5783-5983
observation spacing (km)	100	150	100	100
min. spacecraft altitude (km)	198	212	173	184
max. spacecraf 1 altitude (km)	285	443	380	328
vertical gravity map altitude	250	200	250	200
line-of-sight angle (deg)	72	38	65	80

‘l’able I. Local gravity inversion parameters.

FIGURE CAPTIONS

Figure 1. This Magellan radar image of Bell Regio covers a somewhat smaller area (approximately 22°-38°N, 400-5501?) than the gravity study region. One degree of latitude is equal to -105 km. This and other images are in a sinusoidal equal area projection. North is up. The radar illumination angle is from the left; incidence angles as a function of latitude are given in Pettengill *et al,* (1991). Black bars indicate gaps in the data at the time when the mosaic was made. Most gaps have been filled subsequently. Tepev Mons, with associated flows, is the bright region in the right center of the image. The dark area to the west is another volcanic center whose radar dark flows partially embay an impact crater. The bright annulus at the top of the image is Nefertiti Corona, Two bright, linear, northeast-trending regions of complex ridged terrain intersect with the flows at Tepev Mons.

Figure 2. Magellan radar image of Atla Regio. This is the same region as analyzed in the gravity, minus the northern most five degrees (- 10°S - 20°N, 1820-21 5°E). Three large volcanic edifices are visible. The bright area at the center of the image is Ozza Mons. The elongated dark patch sunrounded by brighter material to the southwest of Ozza Mons is Maat Mons. Sapas Mons is the bright region of radial lineations to the northeast of Ozza and Maat Montes. A series of rifts radiate out from Ozza Mons, with Ganis Chasma to the north and Dali Chasma to the southwest.

Figure 3. This Magellan radar image of Western Eistla Regio(15°-290N, 344°- 12“E) covers has the same east-west extent as the gravity study area, but is 5° shorter in the north and south directions. The volcanic center at the right of the image is Sif Mons. Gula Mons lies to the west. Guor Linea is the rift system to the southwest of Gula Mons. The two large corona to the north of of Sif and Gula Montes are Idem-Kuva and Nissaba. Numerous impact craters are visible.

Figure 4. Magellan radar image of Beta Regio covering approximately the region of 16°-390 N, 272°-295 E. The bright region near the bottom of the image is Theia Mons. Devana Chasma runs north-south out from Theia Mons; Hecate Chasma is to the southwest. The bright region in the upper part of the image is complex ridged terrain, as are many of the other relatively bright areas. Several impact craters are visible.

Figure 5. Model results from local point mass gravity inversion for Bell Regio, as a function of the singular value cut off. The solid line in Fig. 5a is the standard deviation of the model fit to the data, the dashed line shows the relative model covariance. This model has a higher standard deviation than any of the other local inversions. Figure 5b shows the maximum and minimum values of the gravity field calculated at 200 km as a function of the number of singular values retained. The solution breaks down after approximately 400 singular values, indicating that additional singular values are unconstrained by the data.

Figure 6. A contour map of the vertical gravity, in mgals, derived from the local inversion over Bell Regio is shown calculated at an altitude of 2.00 km in Fig. 6a. The inverse model parameters are given in Table 1. Magellan topography, averaged to a 10 spacing, is shown for the same region in Fig. 6b.

Figure 7. A contour map of the vertical gravity (mgals) over Atla Regio from the local inversion is shown at an altitude of 250 km in Fig. 7a, along with the Magellan topography (km) in Fig. 7b.

Figure 8. Gravity and topograhy fields for Western Eistla Regio. The vertical gravity in mgals is from the local inversion, calculated at an altitude of 200 km (Fig.. 8a), along with Magellan topography in km for the same region (Fig. 8b).

Figure 9. The vertical gravity in mgals from the local inversion for Beta Regio is shown at an altitude of 250 km (Fig. 9a), along with Magellan topography in km for the same region (Fig. 9b). The gravity and topography are not as highly correlated as in many other regions.

Figure 10. Admittance and coherence spectra for Bell Regio from both the local inverion (using GASP) and the spherical harmonic model (Konopliv and Sjogren 1994). There is a vertical offset of 10 mgals/km between the two spectra. The source of the offset is unknown (see discussion in the text); 10 mgals/km was added to the. spectrum for the local, inversion to bring it into agreement with the spherical harmonic model. The free air admittance spectra are compared to models of local, isostatic compensation at depths of 25, 50, 100, and 150 km in Fig. 10c. 'I'he Bouger gravity admittance spectra is compared with a model of isostatic compensation with surface and subsurface loading and a combination of the two in Fig. 10b. Figure 10c shows compares the free air gravity spectra to the hotspot model, where dashed lines indicate top loading, and solid lines are for the long wavelength, bottom-loaded portion of the hotspot model (see text). The same model is shown in Fig. 10d, but with a crustal thickness of 50 km to illustrate the sensitivity of other parameters to the choice of crustal thickness. Figure 10e shows the coherence spectra and models of flexural compensation (Forsyth 1985) for an effective elastic thickness of 52 km and various ratios of bottom-to-top loading. The fit to these models is discussed in the text.

Figure 11, Admittance spectra for Atla Regio are compared to models of local compensation (Fig. 11a), local and regional compensation (Fig. 1 lb), and hotspot compensation (Fig. 1 1c), as in Fig. 10. A loading model is also fit to the coherence spectra (Fig. 1 id).

Figure 12. Admittance spectra for Western Eistla Regio are compared to models of local compensation (Fig. 12a), local and regional compensation (Fig. 12b), and hotspot compensation (Fig. 12c), as in Fig. 10. The coherence spectra is also compared to a flexural compensation model (Fig. 12d).

Figure 13. Admittance spectra for Beta Regio are compared to models of local compensation (Fig. 13a), local and regional compensation (Fig. 13b), and hotspot compensation (Fig. 13c), as in Fig. 10. The coherence spectra is also compared to a flexural compensation model (Fig. 13d).

Figure 1

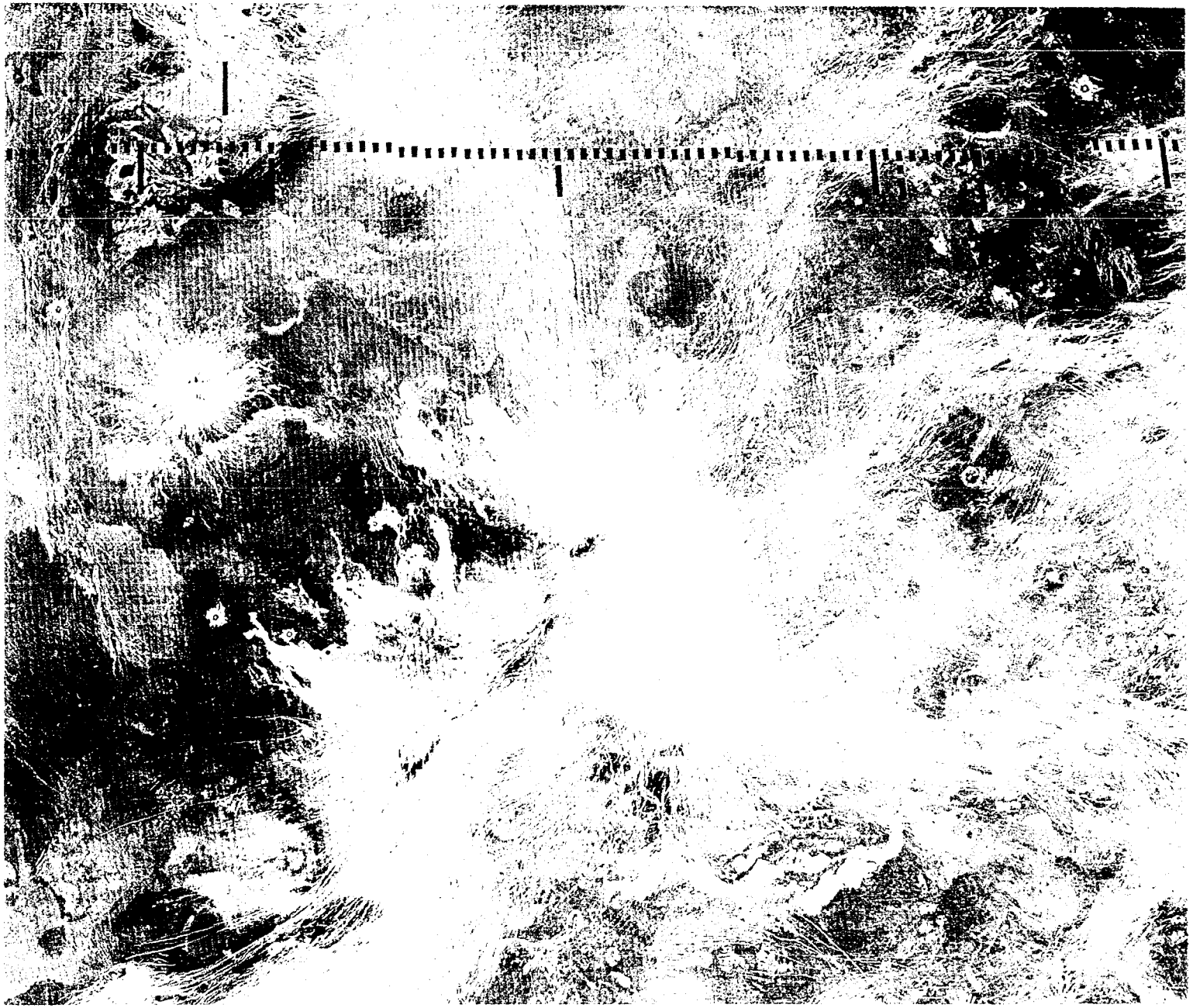

Figure 2

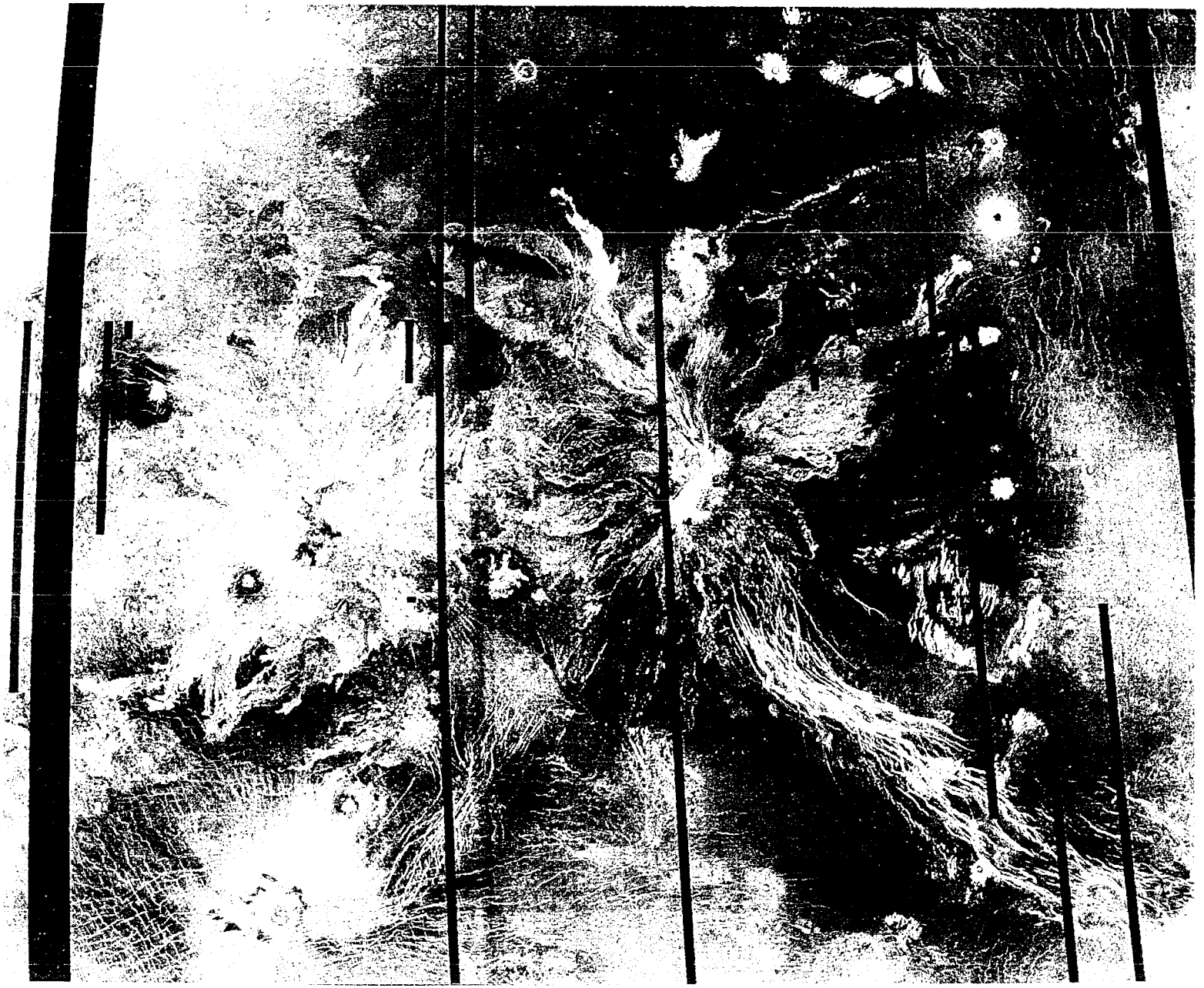

Figure 3

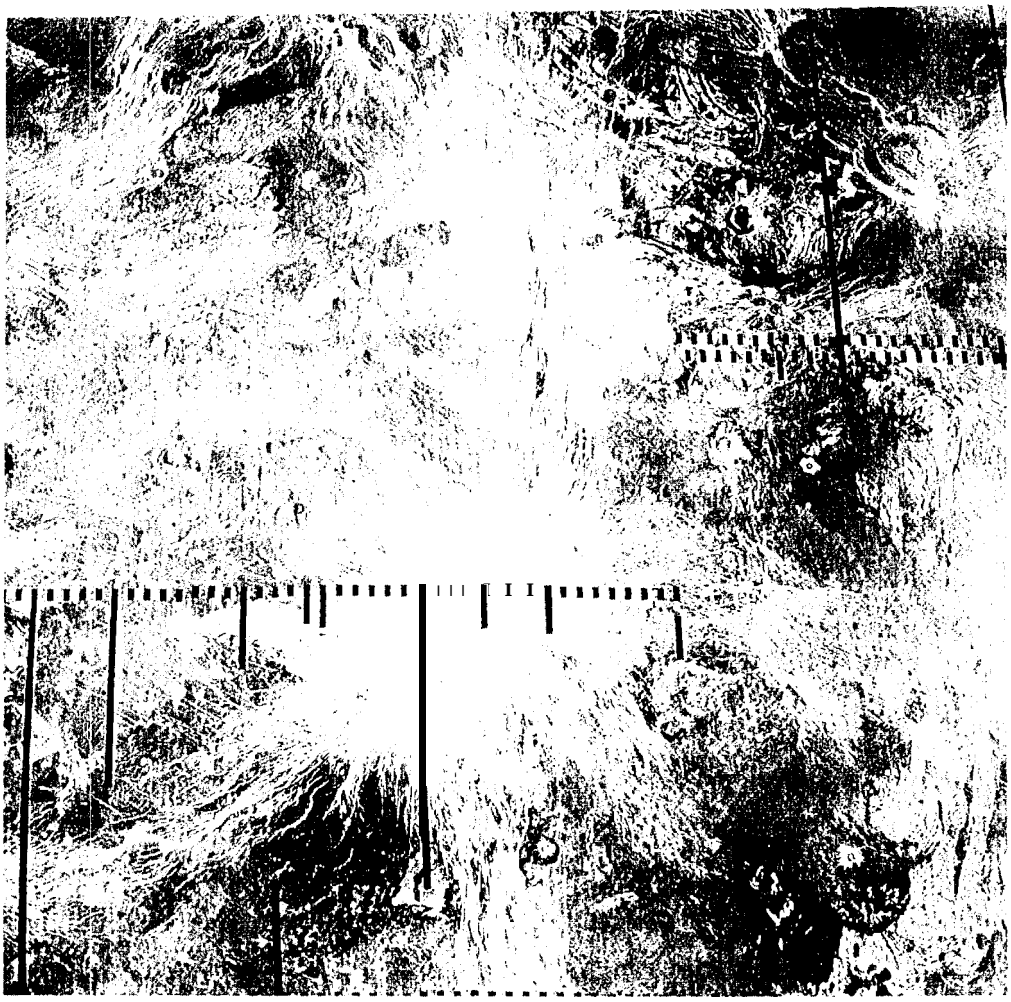

Figure 4

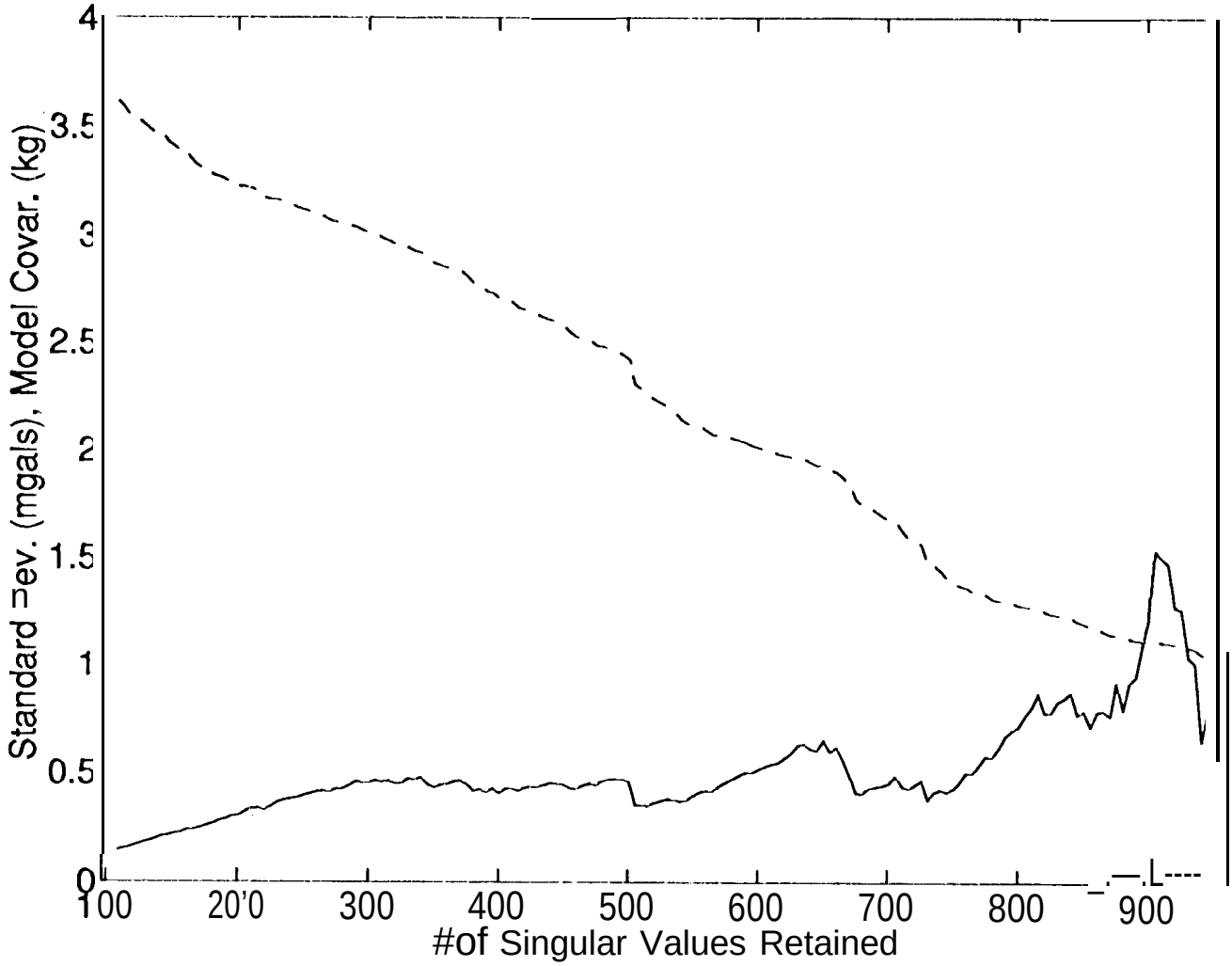
Standard Dev. (mgals), Model Covar. (kg)
4
3.5
3
2.5
2
1.5
1
0.5
0
100
200
300
400
500
600
700
800
900
#of Singular Values Retained

Figure 5a

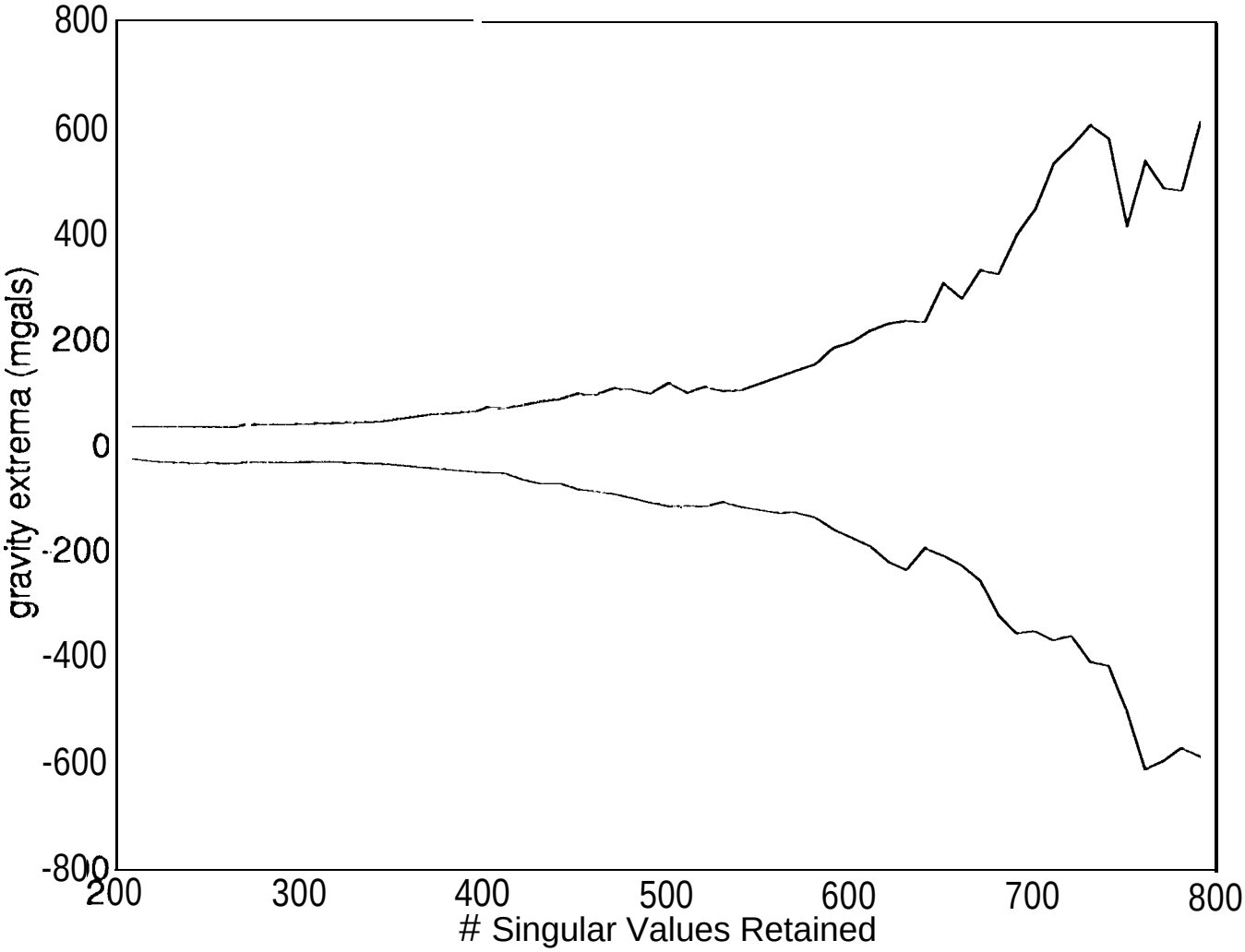
800
600
400
200
0
-200
-400
-600
-800
gravity extrema (mgals)
200
300
400
500
600
700
800
Singular Values Retained

Figure 5b

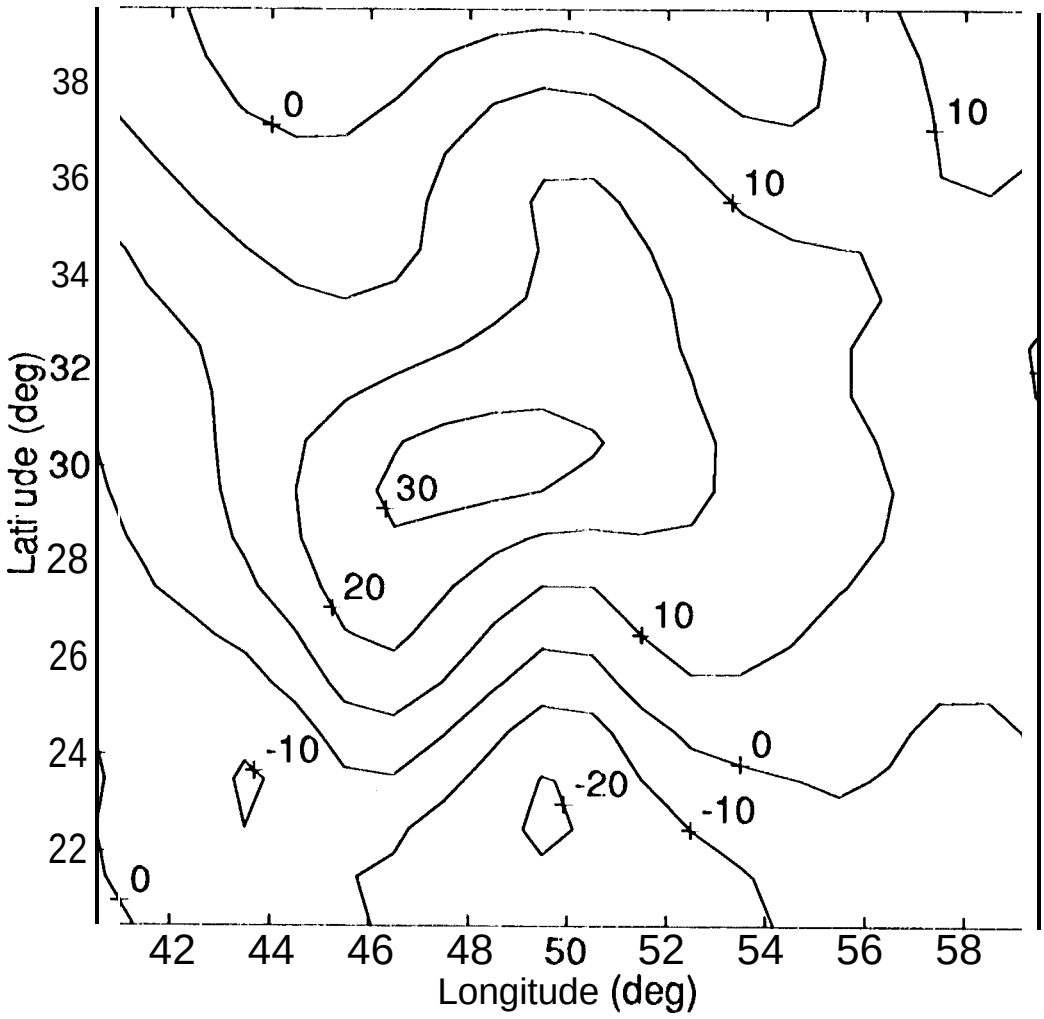
38
36
34
32
30
28
26
24
22
Latitude (deg)
42
44
46
48
50
52
54
56
58
Longitude (deg)
0
10
10
30
20
10
0
-10
-20
-10
0

Figure 6a

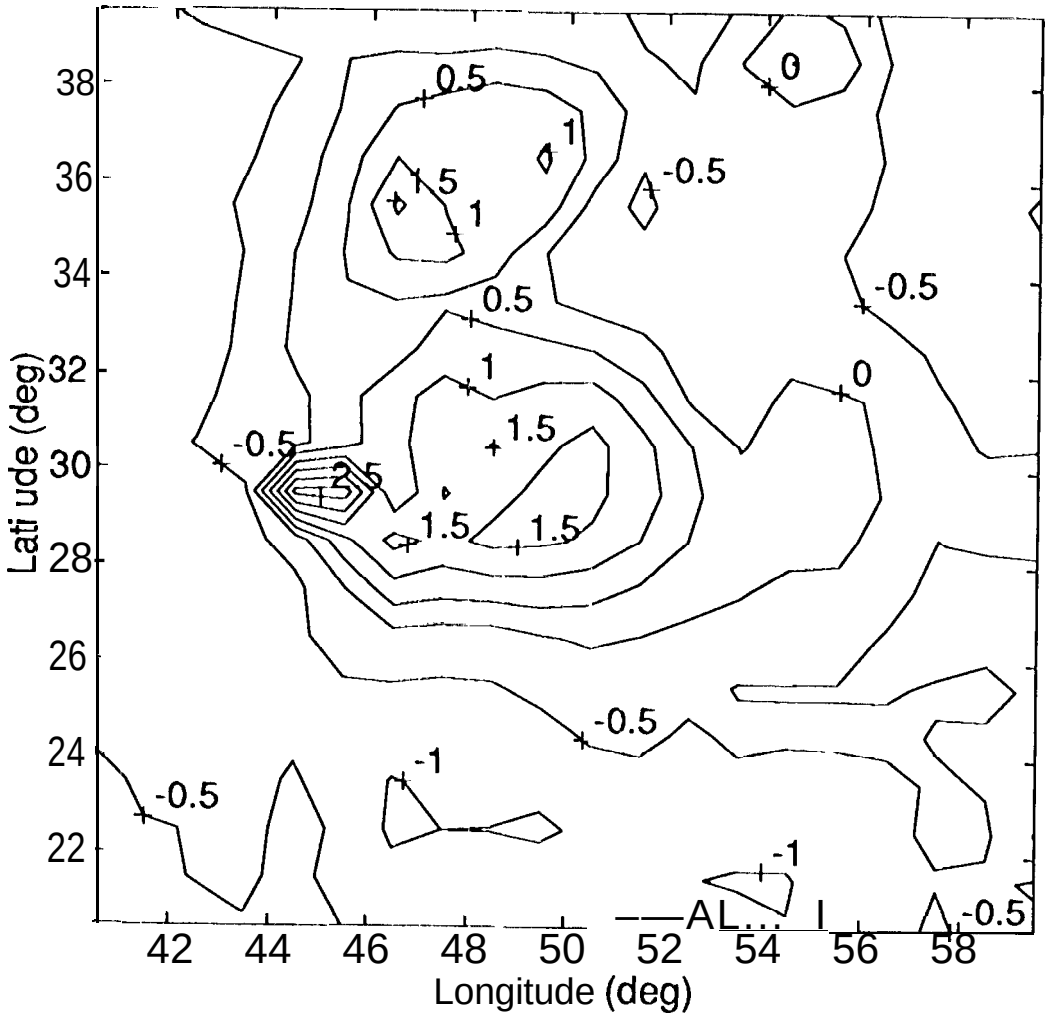
Lati ude (deg)
Longitude (deg)
38
36
34
32
30
28
26
24
22
42
44
46
48
50
52
54
56
58
0.5
1
1.5
-0.5
0
-1

Fi gure 6b

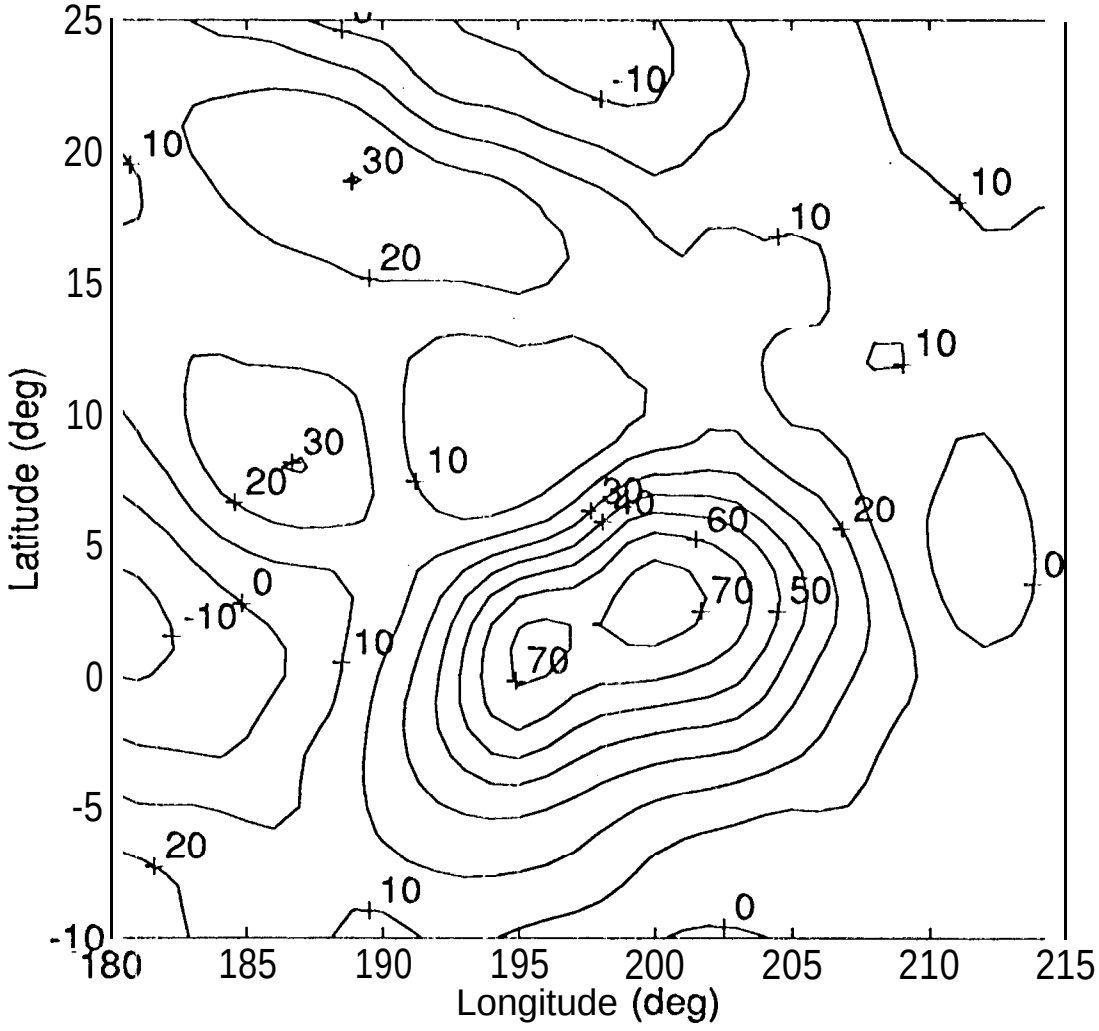
25
20
15
10
5
0
-5
-10
Latitude (deg)
180
185
190
195
200
205
210
215
Longitude (deg)
-10
10
30
20
10
10
10
30
20
30
40
60
20
0
0
-10
10
70
50
70
20
10
0

Figure 7a

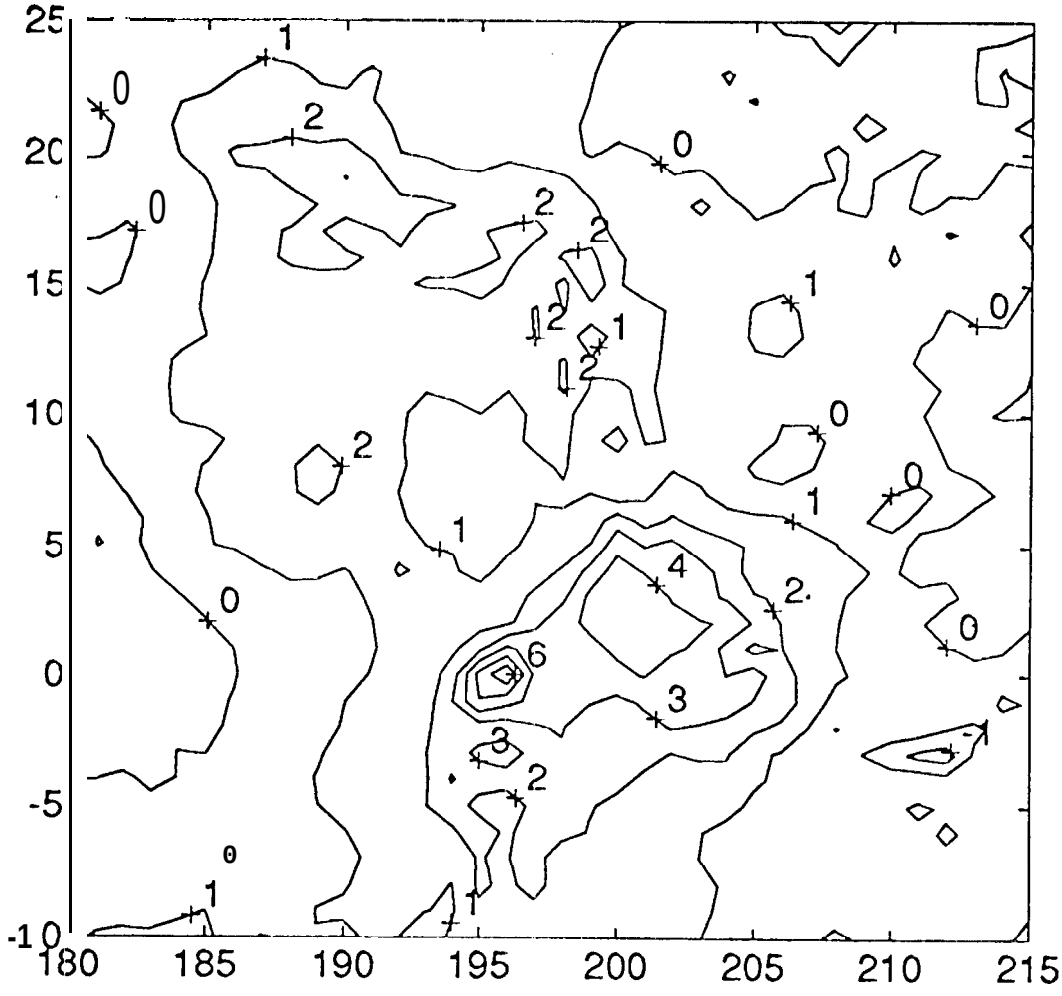

Figure 7b

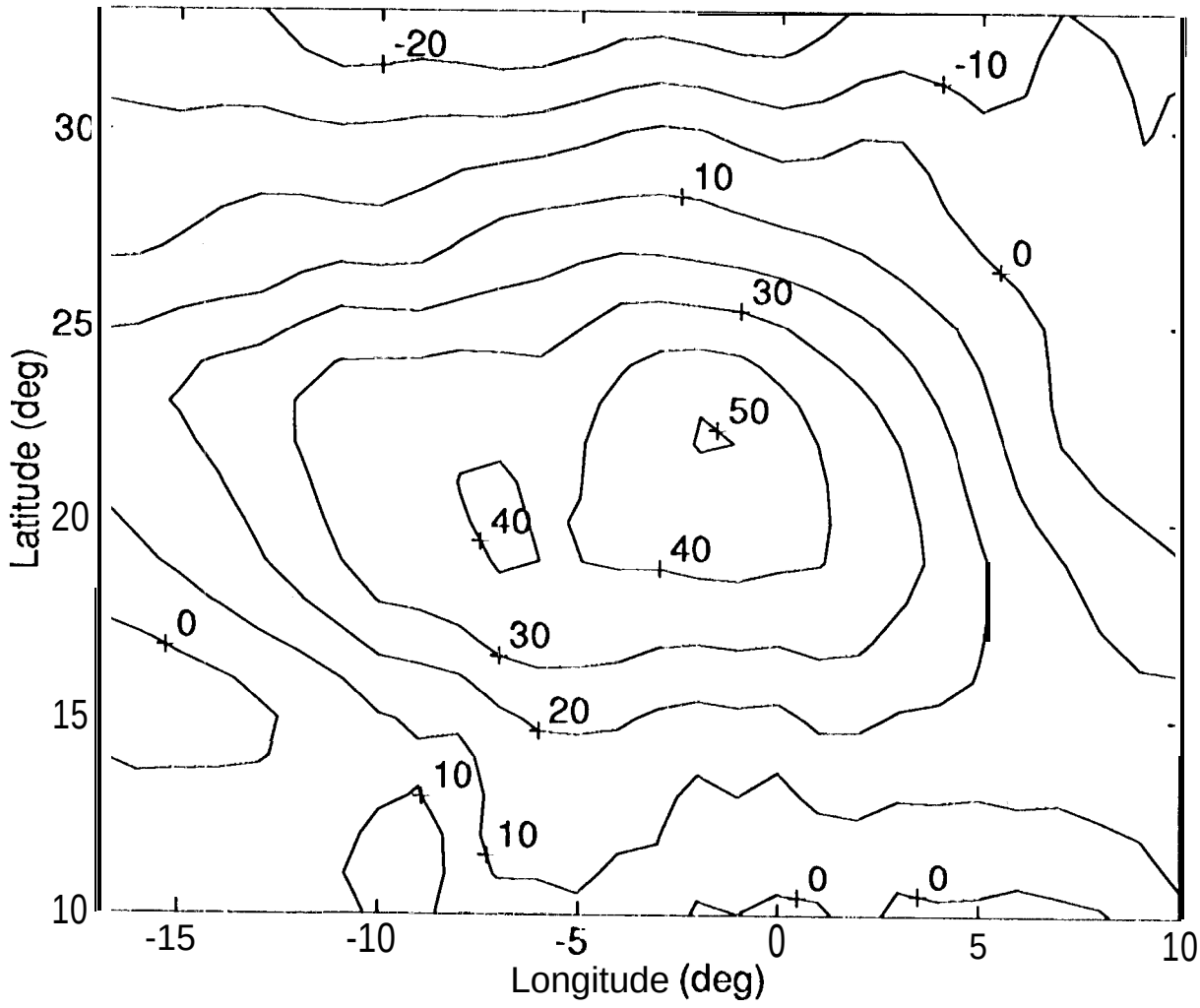
-20
-10
10
0
30
50
40
40
30
20
0
10
10
0
0
30
25
20
15
10
Latitude (deg)
-15
-10
-5
0
5
10
Longitude (deg)

Figure 8a

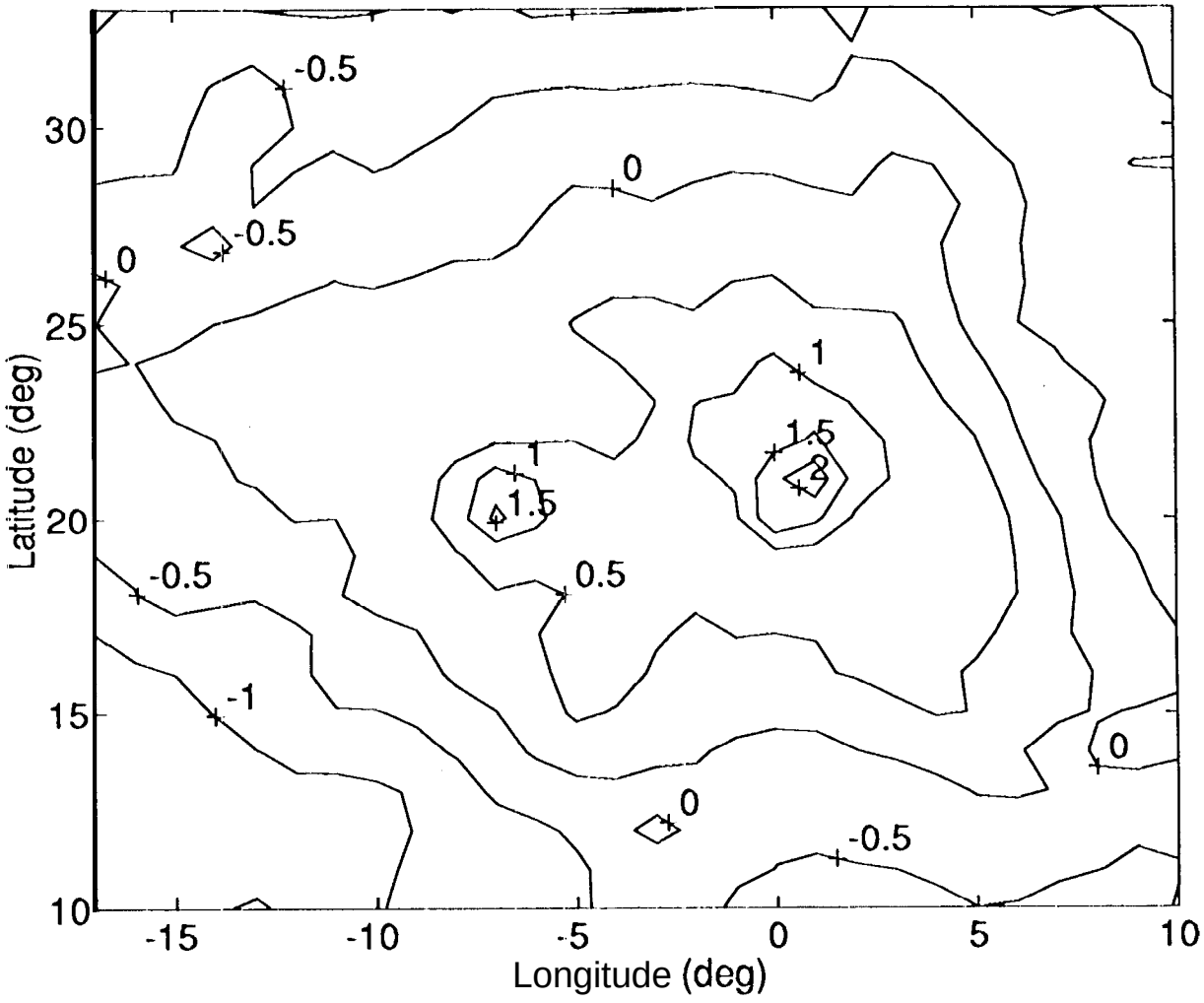
-0.5
0
-0.5
0
1
1.5
1
1.5
0.5
-0.5
-1
0
0
-0.5
30
25
20
15
10
-15
-10
-5
0
5
10
Latitude (deg)
Longitude (deg)

Figure 8b

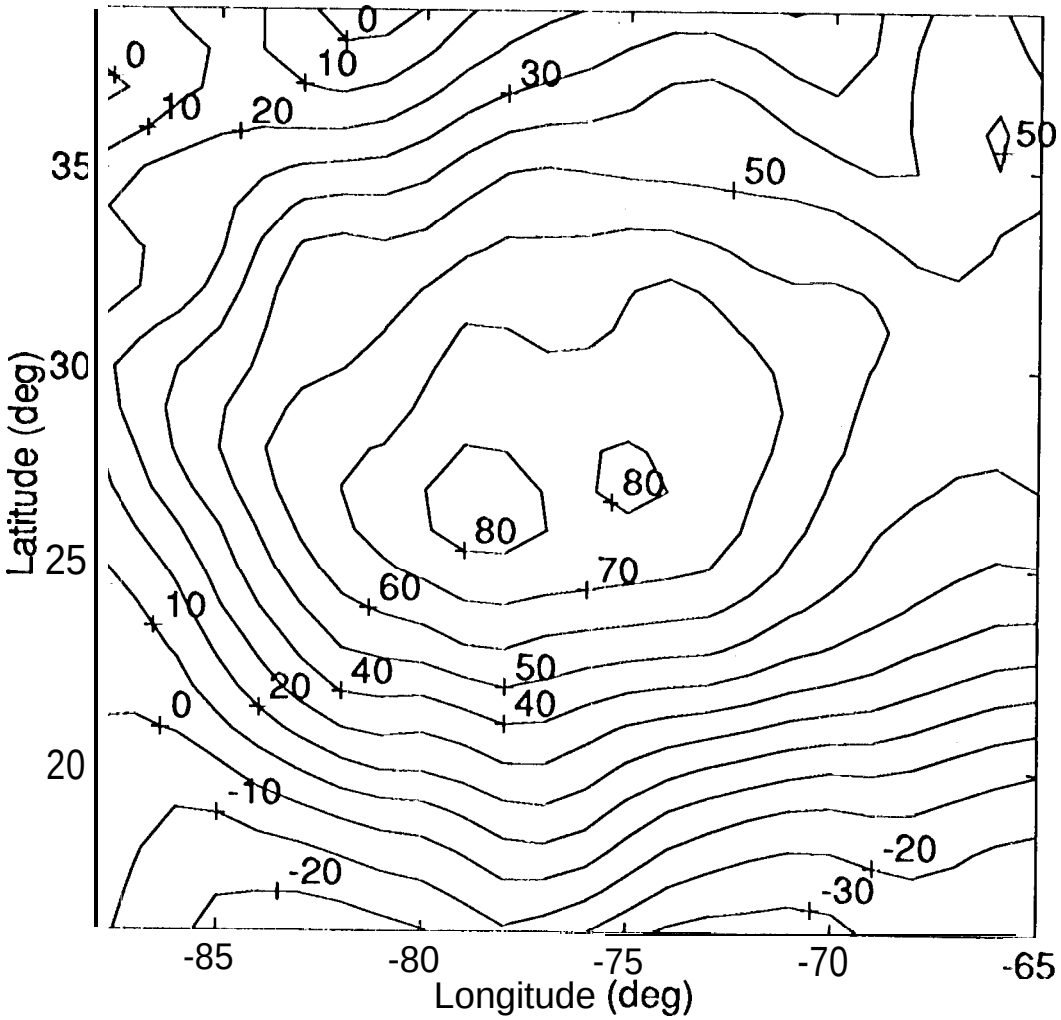
Latitude (deg)
35
30
25
20
-85
-80
-75
-70
-65
Longitude (deg)
0
10
20
30
50
80
70
60
40
-10
-20
-30

Figure 9a

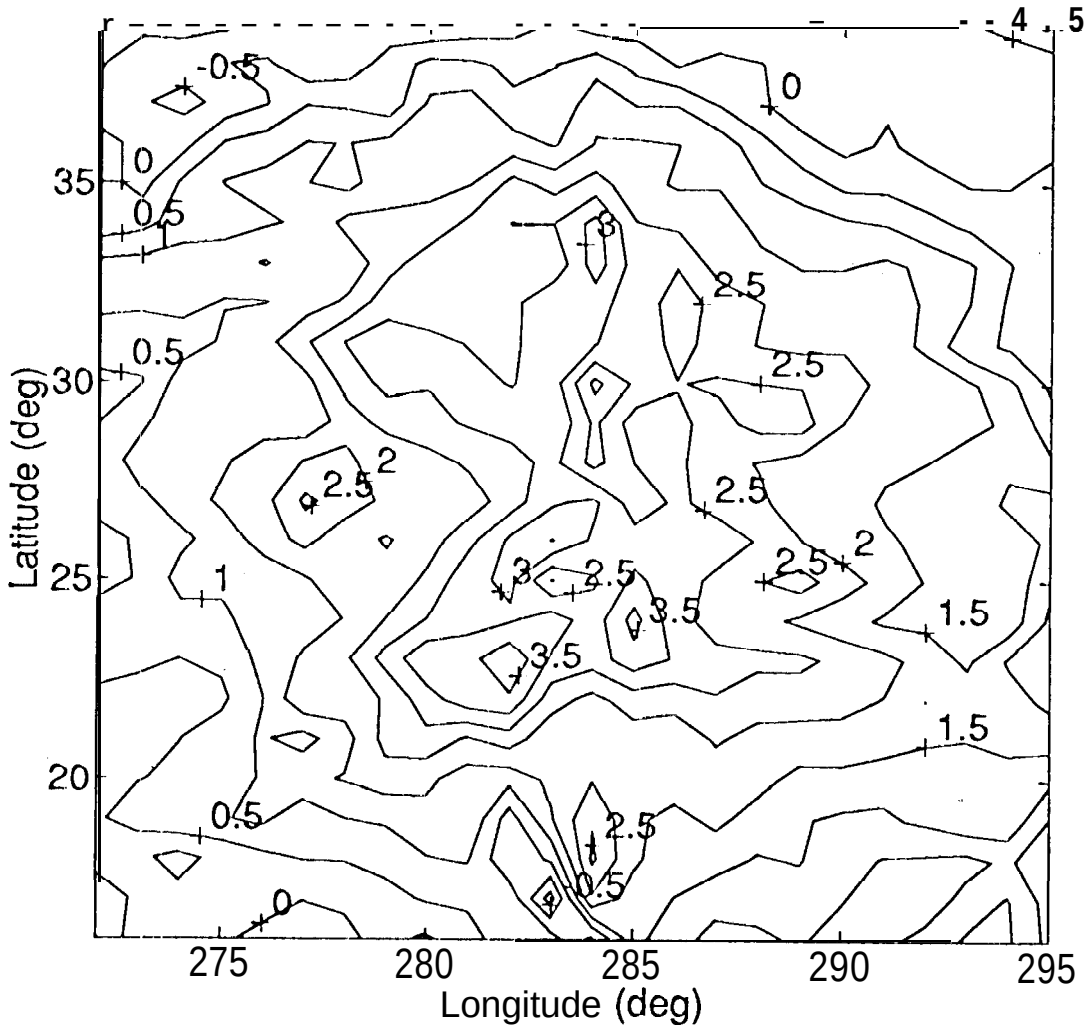
Latitude (deg)
Longitude (deg)
35
30
25
20
275
280
285
290
295
-0.5
0
0.5
1
1.5
2
2.5
3
3.5
4
5

Figure **9 b**

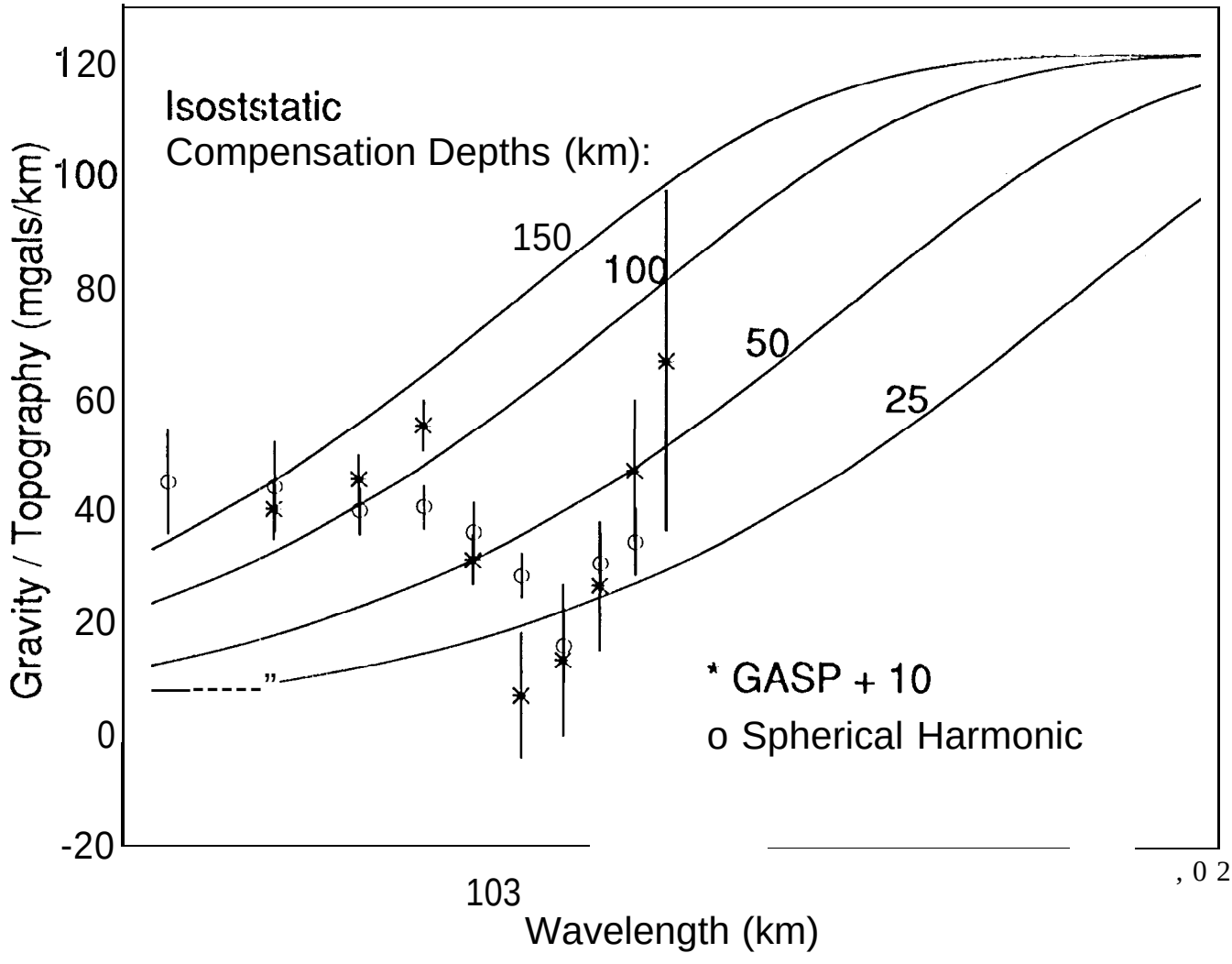
120
100
80
60
40
20
0
-20
Gravity / Topography (mgals/km)
Isoststatic
Compensation Depths (km):
150
100
50
25
* GASP + 10
o Spherical Harmonic
, 0 2
103
Wavelength (km)

Figure 10a

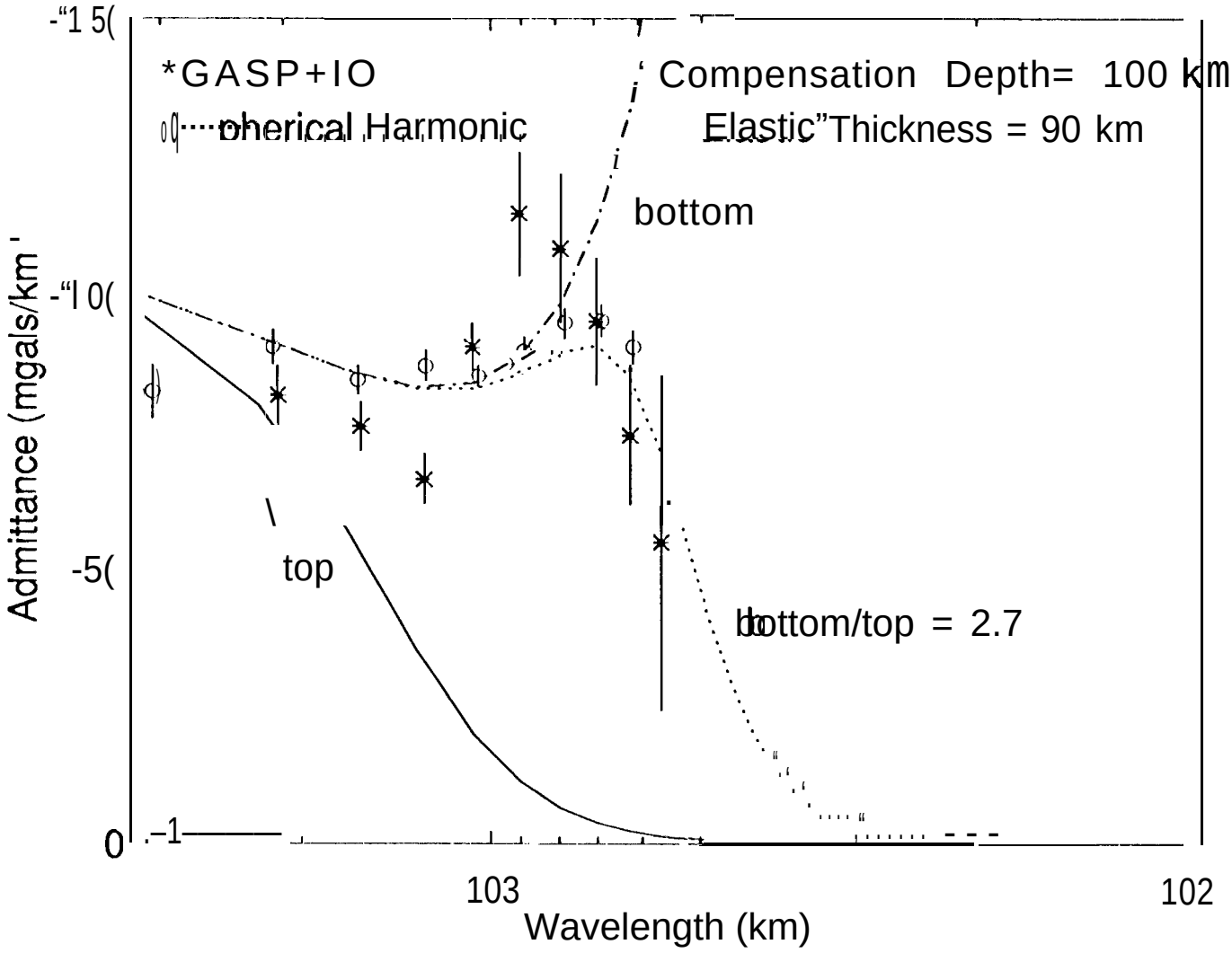
*GASP+IO
Spherical Harmonic
Compensation Depth= 100 km
Elastic Thickness = 90 km
bottom
top
bottom/top = 2.7
Admittance (mgals/km)
103
102
Wavelength (km)

Figure 10b

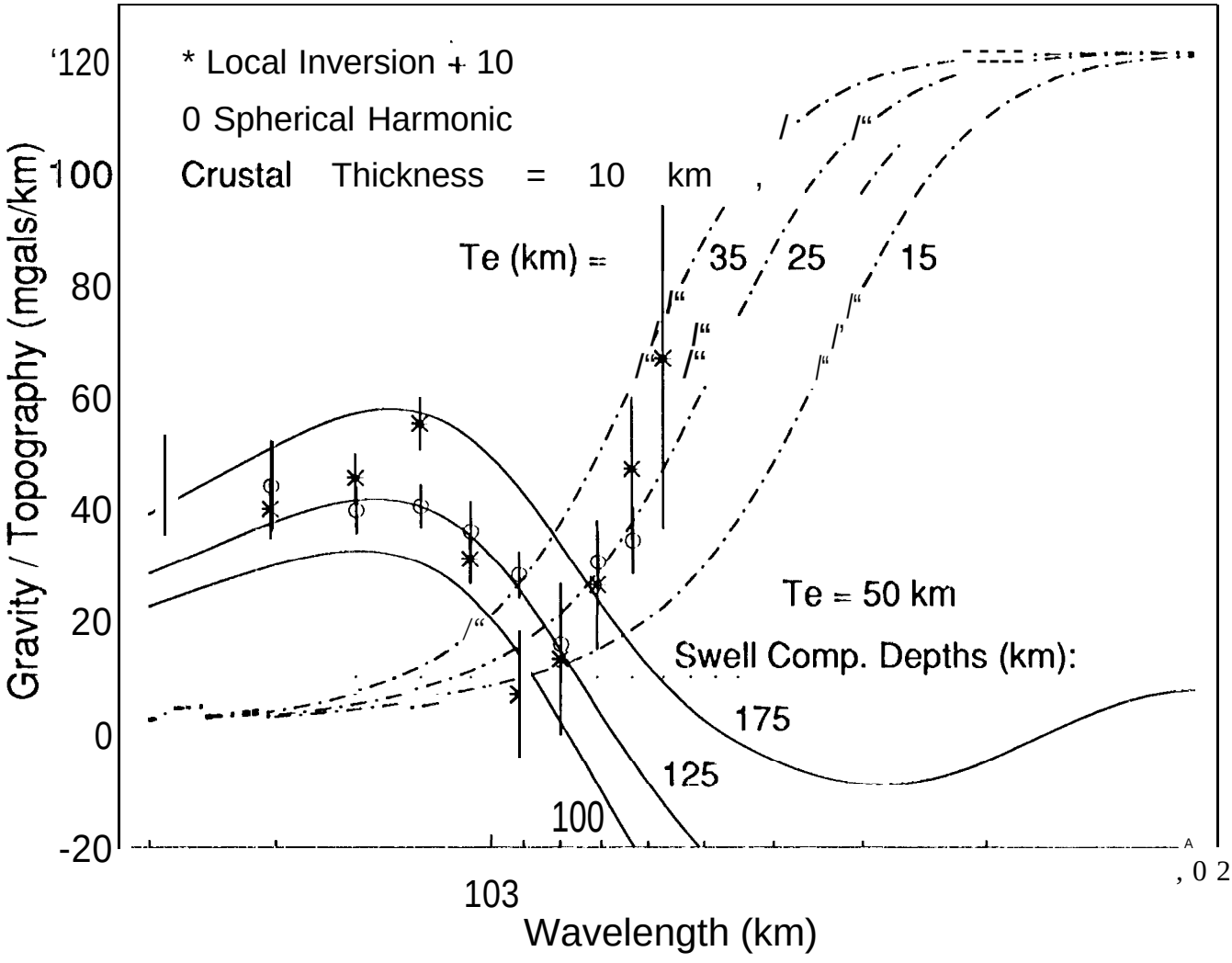
* Local Inversion + 10
0 Spherical Harmonic
Crustal Thickness = 10 km
Te (km) = 35 25 15
Te = 50 km
Swell Comp. Depths (km):
175
125
100
Gravity / Topography (mgals/km)
120
100
80
60
40
20
0
-20
103
Wavelength (km)

Figure 10c

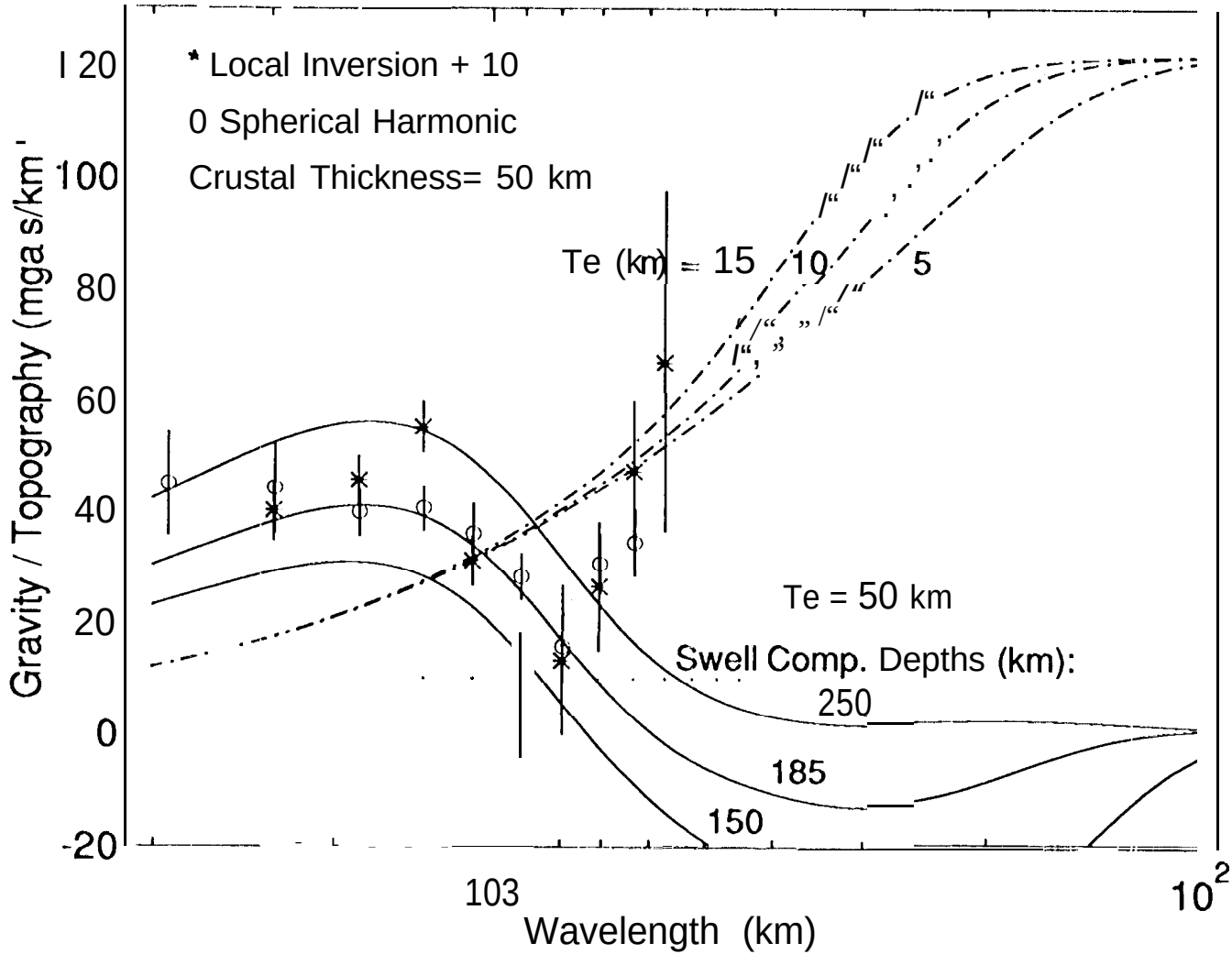
* Local Inversion + 10
0 Spherical Harmonic
Crustal Thickness= 50 km
Te (km) = 15 10 5
Te = 50 km
Swell Comp. Depths (km):
250
185
150
Gravity / Topography (mga s/km'
I 20
100
80
60
40
20
0
-20
103
10^2
Wavelength (km)

Figure 10d

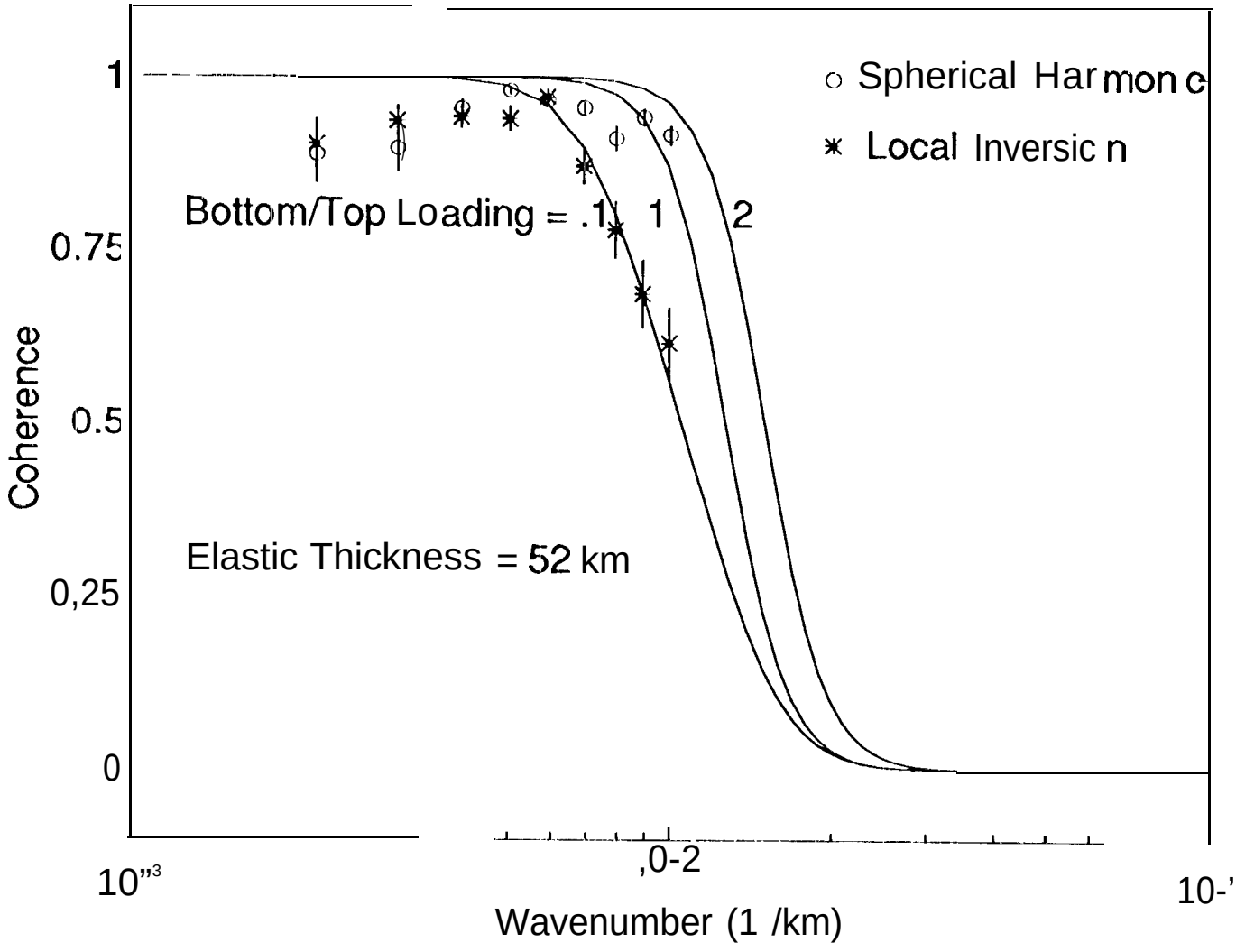
1
0.75
0.5
0,25
0
Coherence
Spherical Harmonic
Local Inversion
Bottom/Top Loading = .1
1
2
Elastic Thickness = 52 km
10"3
,0-2
10-'
Wavenumber (1 /km)

Figure 10e

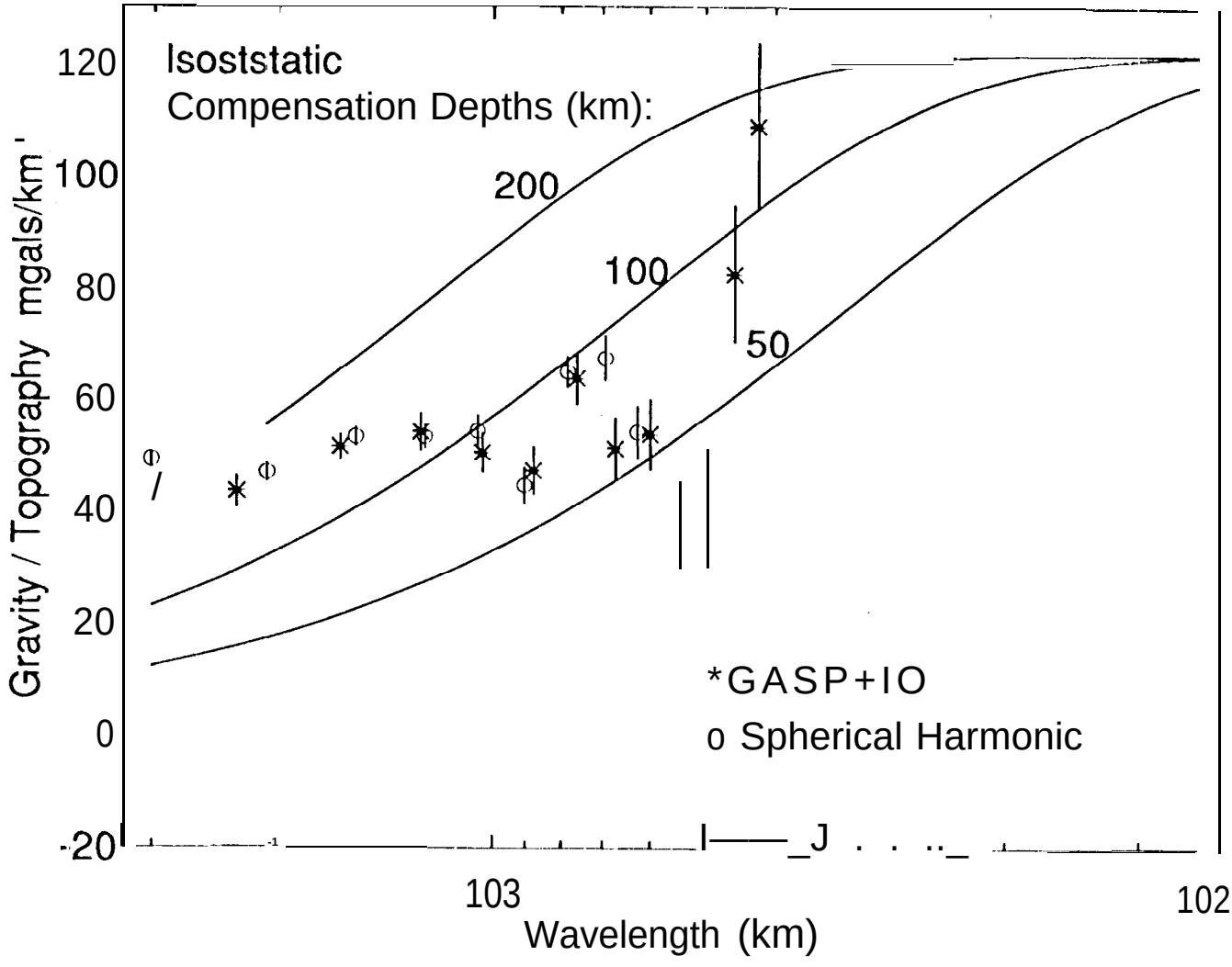
Isoststatic
Compensation Depths (km):
200
100
50
*GASP+IO
o Spherical Harmonic
Gravity / Topography mgals/km'
120
100
80
60
40
20
0
-20
103
102
Wavelength (km)

Figure 11 a

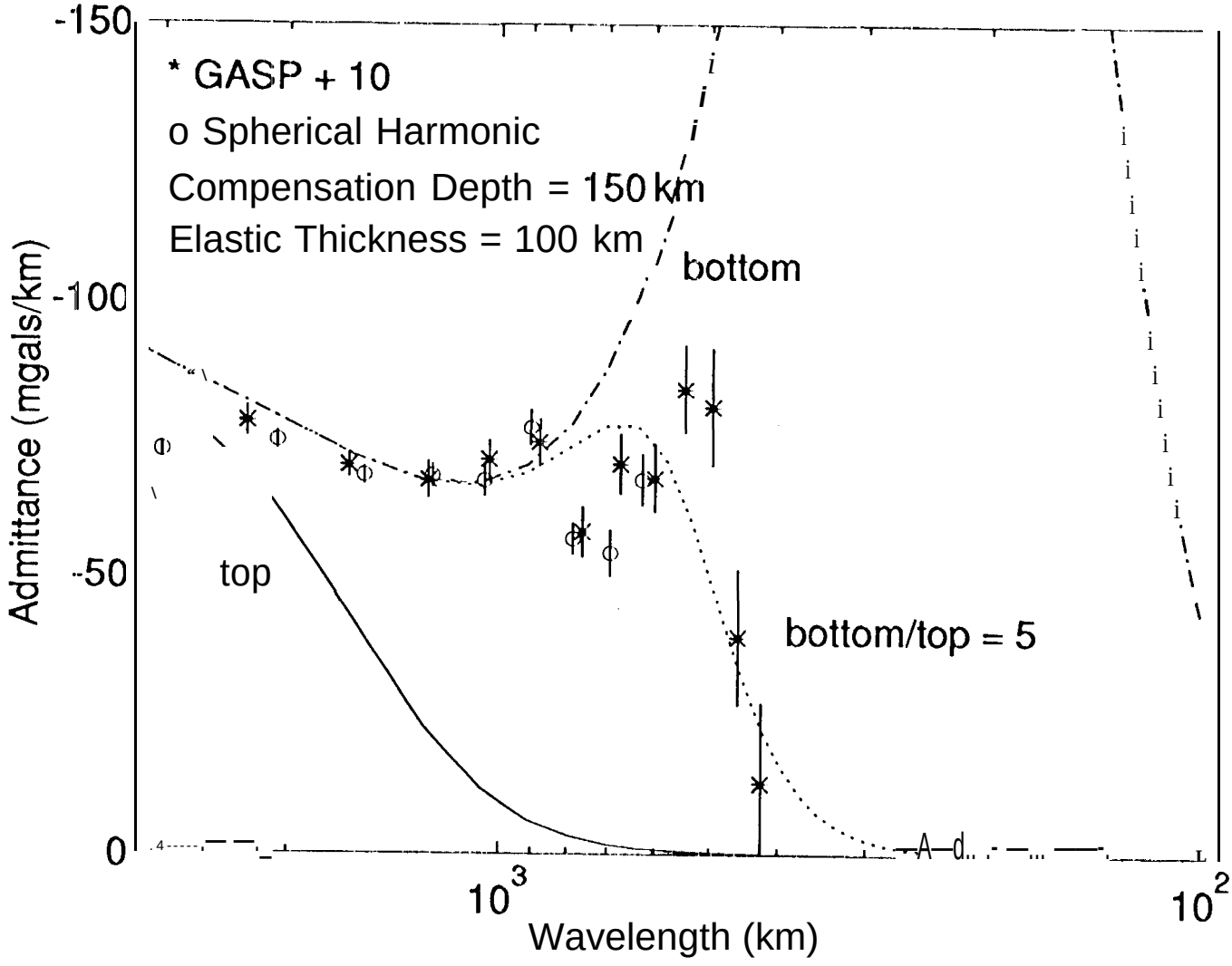
-150
-100
-50
0
Admittance (mgals/km)
* GASP + 10
o Spherical Harmonic
Compensation Depth = 150 km
Elastic Thickness = 100 km
bottom
top
bottom/top = 5
10^3
10^2
Wavelength (km)

Figure 1 lb

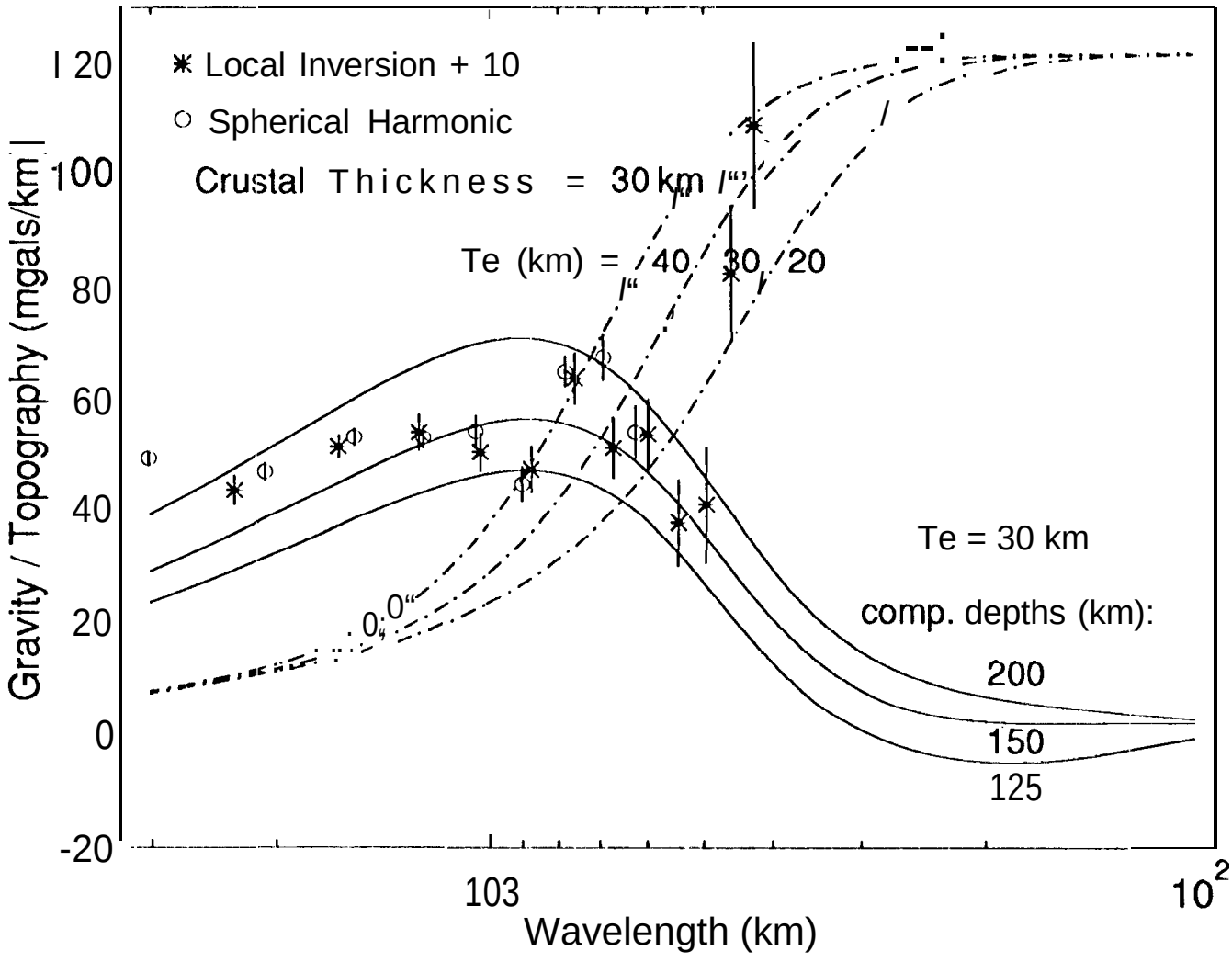
Local Inversion + 10
Spherical Harmonic
Crustal Thickness = 30 km
Te (km) = 40 30 20
Te = 30 km
comp. depths (km):
200
150
125
Gravity / Topography (mgals/km)
120
100
80
60
40
20
0
-20
103
10^2
Wavelength (km)

Figure 11c

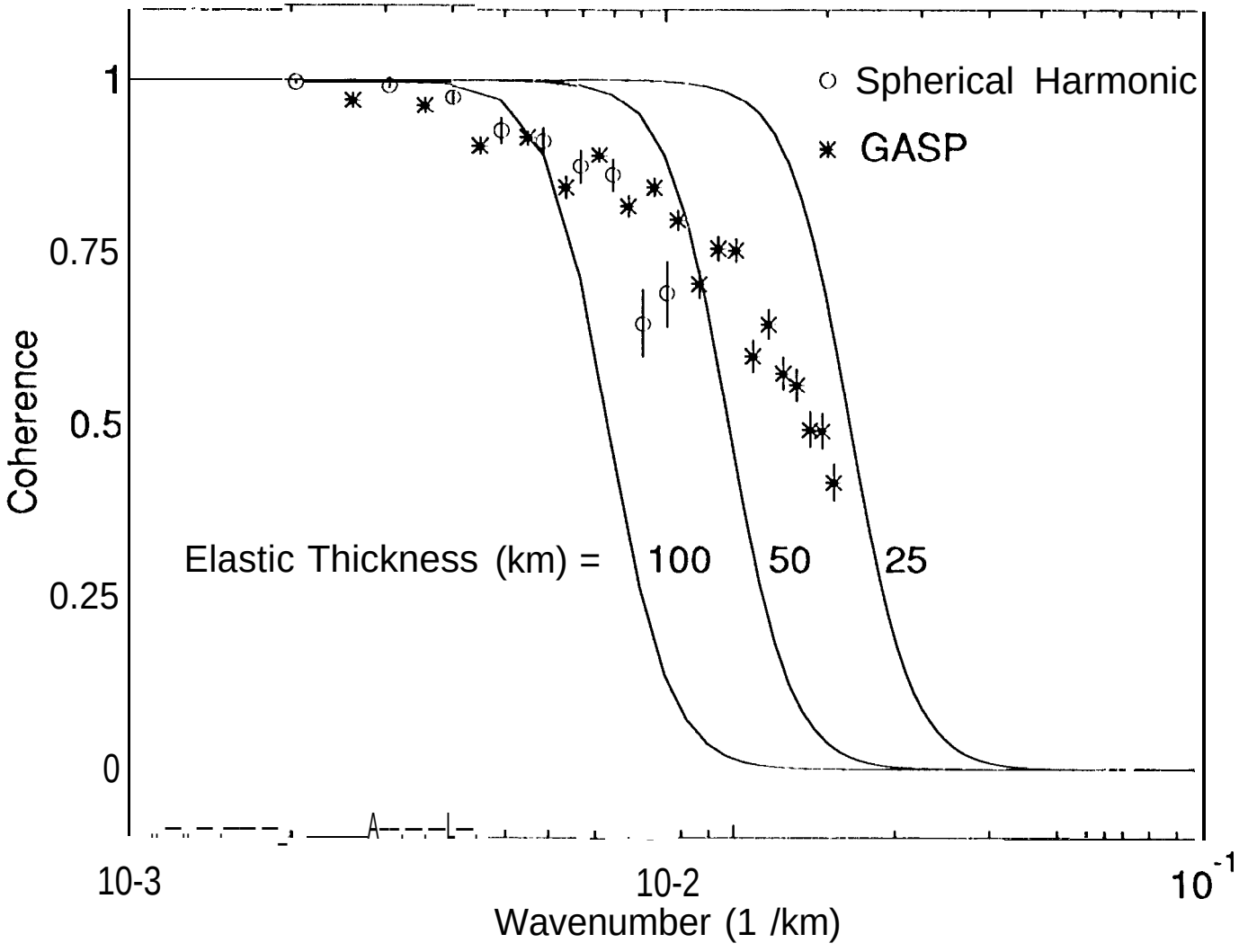
1
0.75
0.5
0.25
0
Coherence
Spherical Harmonic
GASP
Elastic Thickness (km) =
100
50
25
10-3
10-2
10-1
Wavenumber (1 /km)

Figure 11d

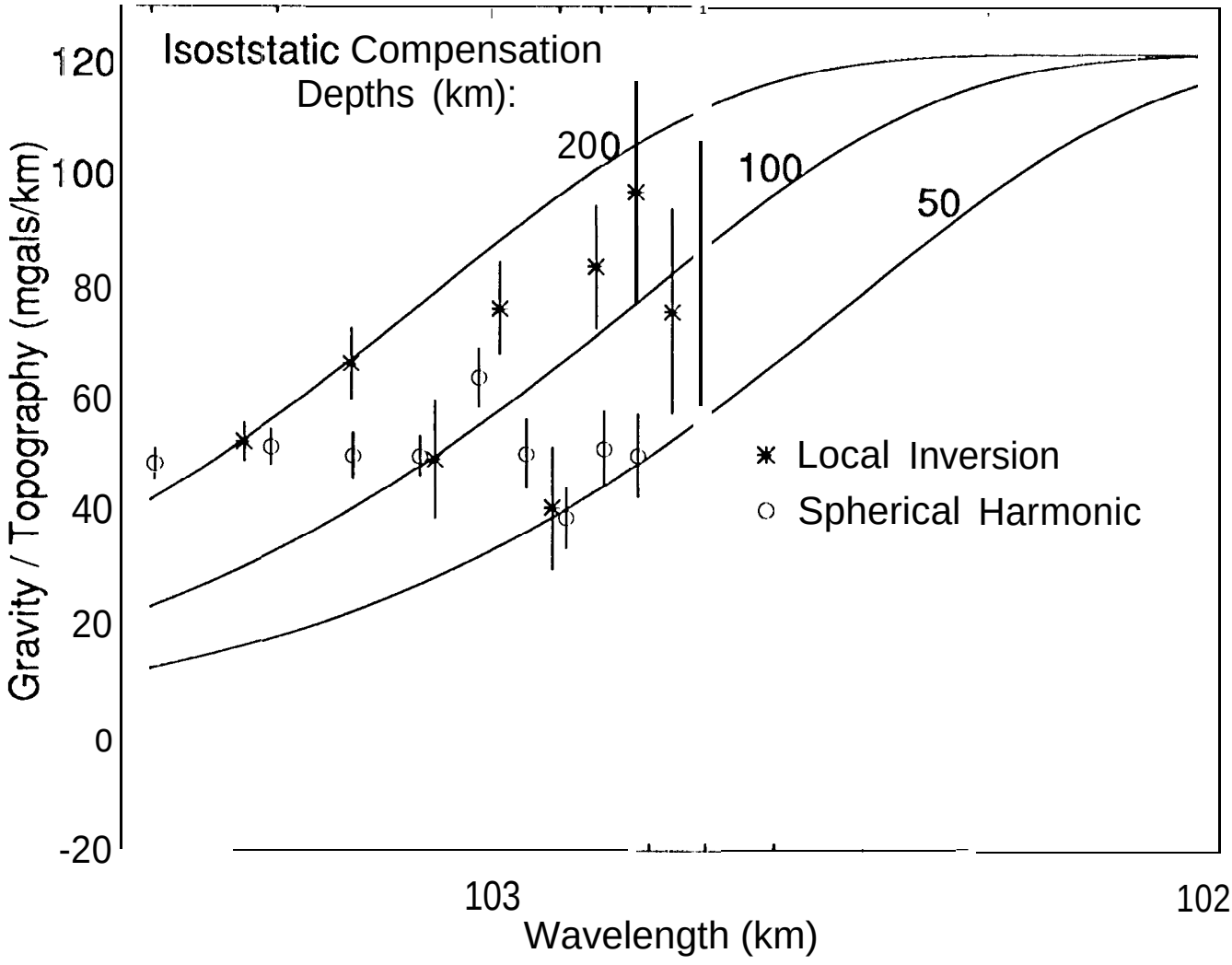
Isoststatic Compensation
Depths (km):
200
100
50
Local Inversion
Spherical Harmonic
Gravity / Topography (mgals/km)
120
100
80
60
40
20
0
-20
103
102
Wavelength (km)

Figure 12a

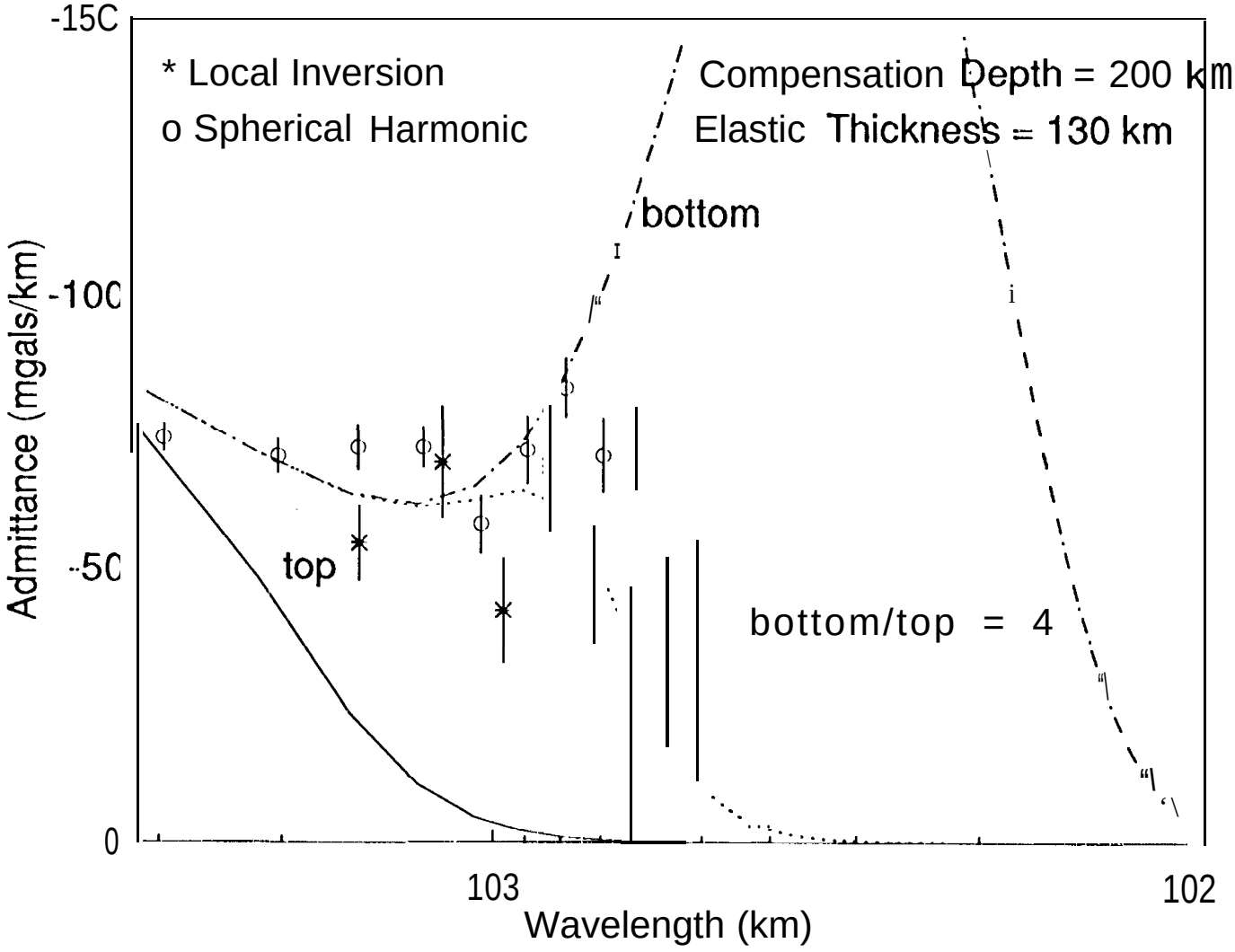
-15C
-100
-50
0
* Local Inversion
o Spherical Harmonic
Compensation Depth = 200 km
Elastic Thickness = 130 km
bottom
top
bottom/top = 4
Admittance (mgals/km)
103
102
Wavelength (km)

Figure 12b

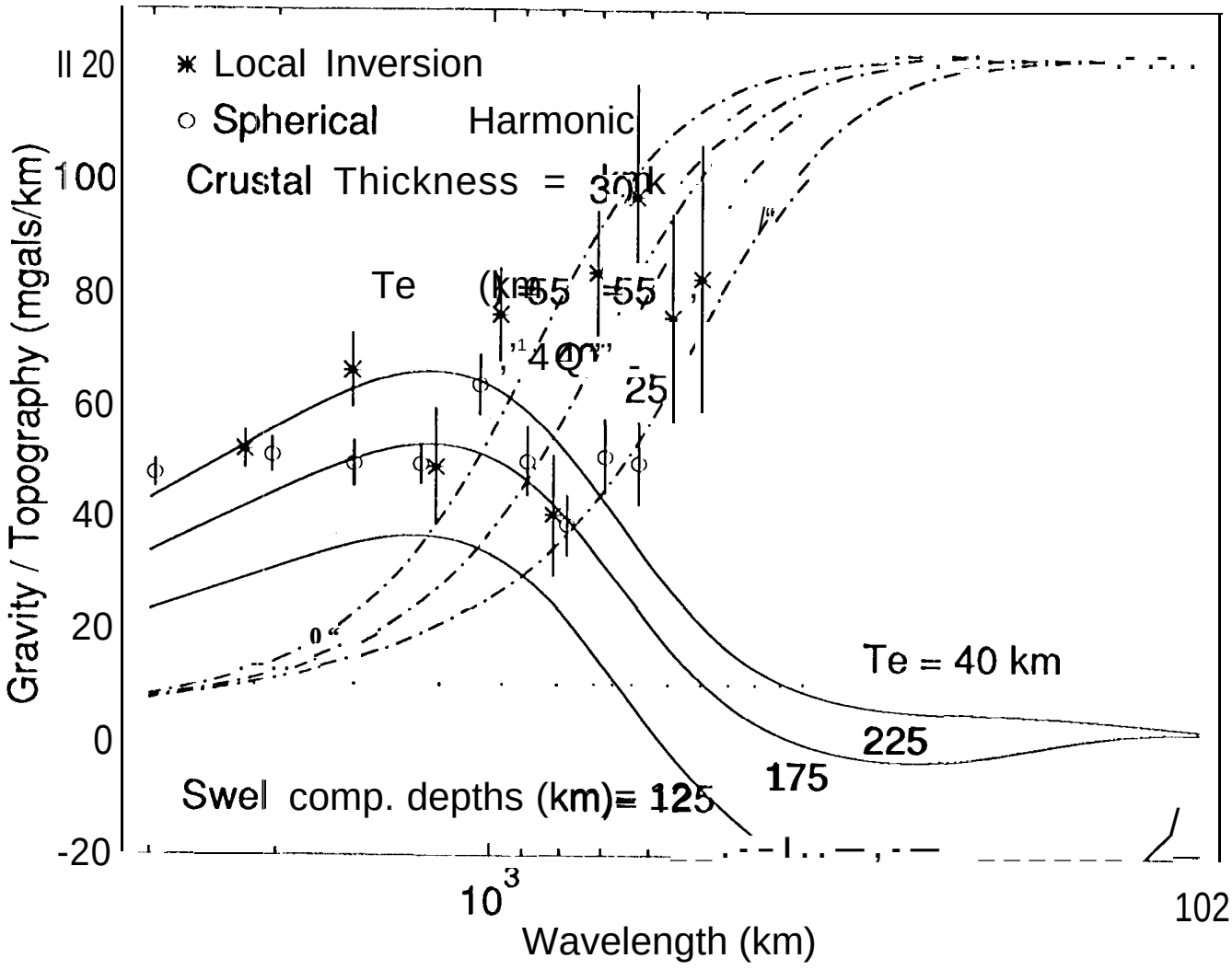
* Local Inversion
○ Spherical Harmonic
Crustal Thickness = 30 km
Te (km) = 55
40
25
0
Te = 40 km
225
175
Swel comp. depths (km) = 125
Gravity / Topography (mgals/km)
120
100
80
60
40
20
0
-20
10^3
102
Wavelength (km)

Figure 12c

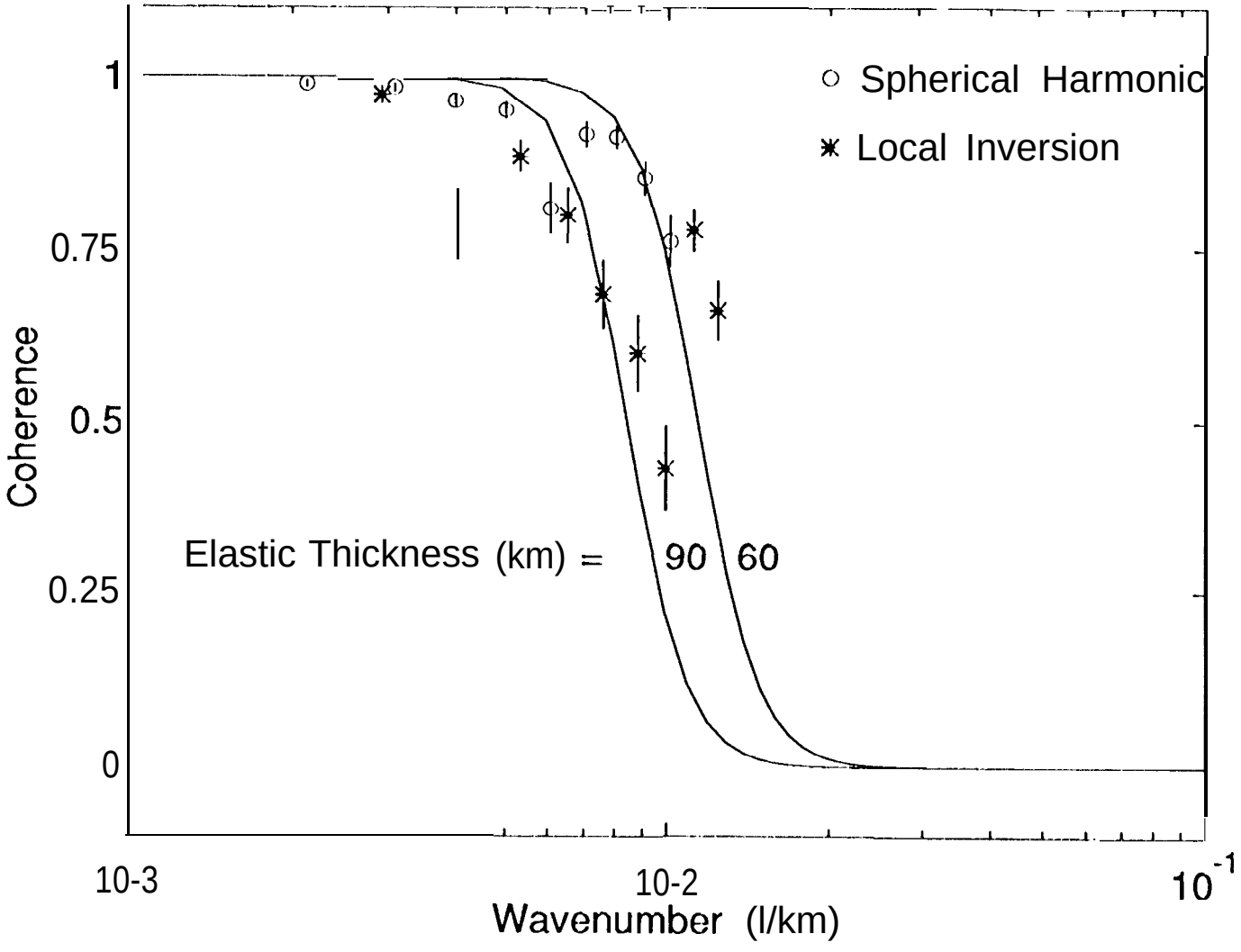
1
0.75
0.5
0.25
0
Coherence
Spherical Harmonic
Local Inversion
Elastic Thickness (km) = 90 60
10-3
10-2
10-1
Wavenumber (l/km)

Figure 12d

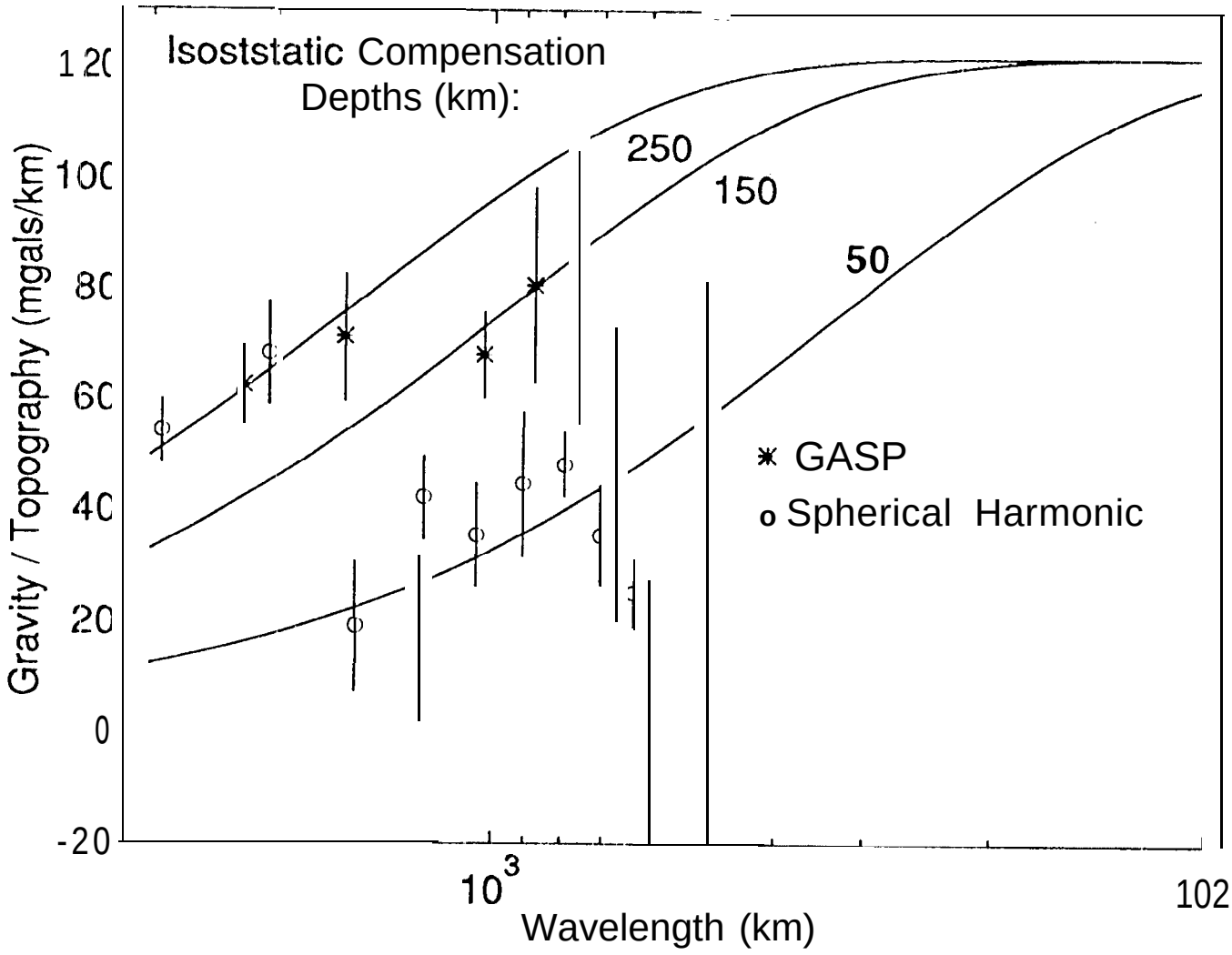
Isoststatic Compensation
Depths (km):
250
150
50
* GASP
o Spherical Harmonic
Gravity / Topography (mgals/km)
120
100
80
60
40
20
0
-20
10^3
102
Wavelength (km)

Figure 13a

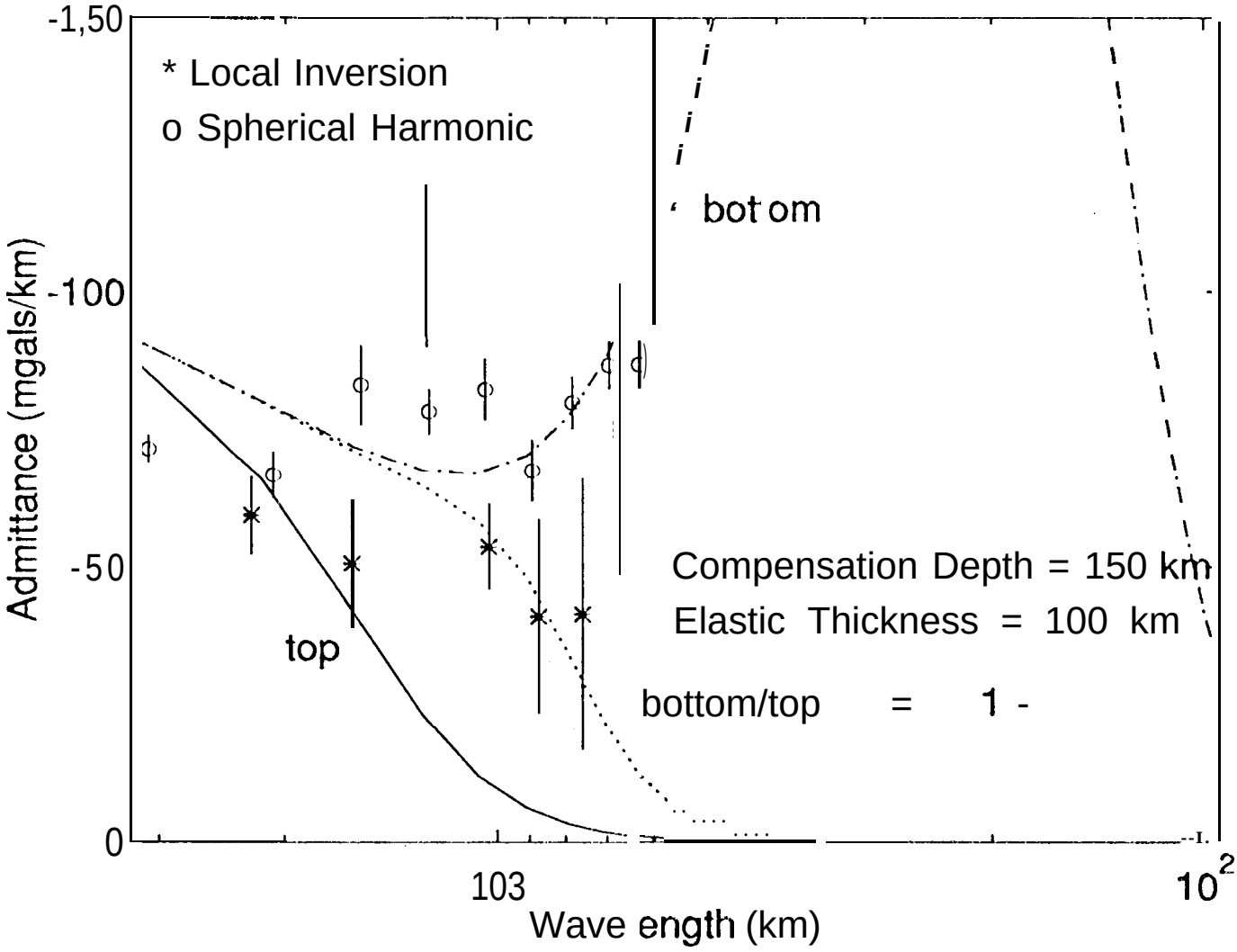
-1,50
-100
-50
0
Admittance (mgals/km)
* Local Inversion
o Spherical Harmonic
bot om
top
Compensation Depth = 150 km
Elastic Thickness = 100 km
bottom/top = 1 -
103
10^2
Wave engtn (km)

Figure 13b

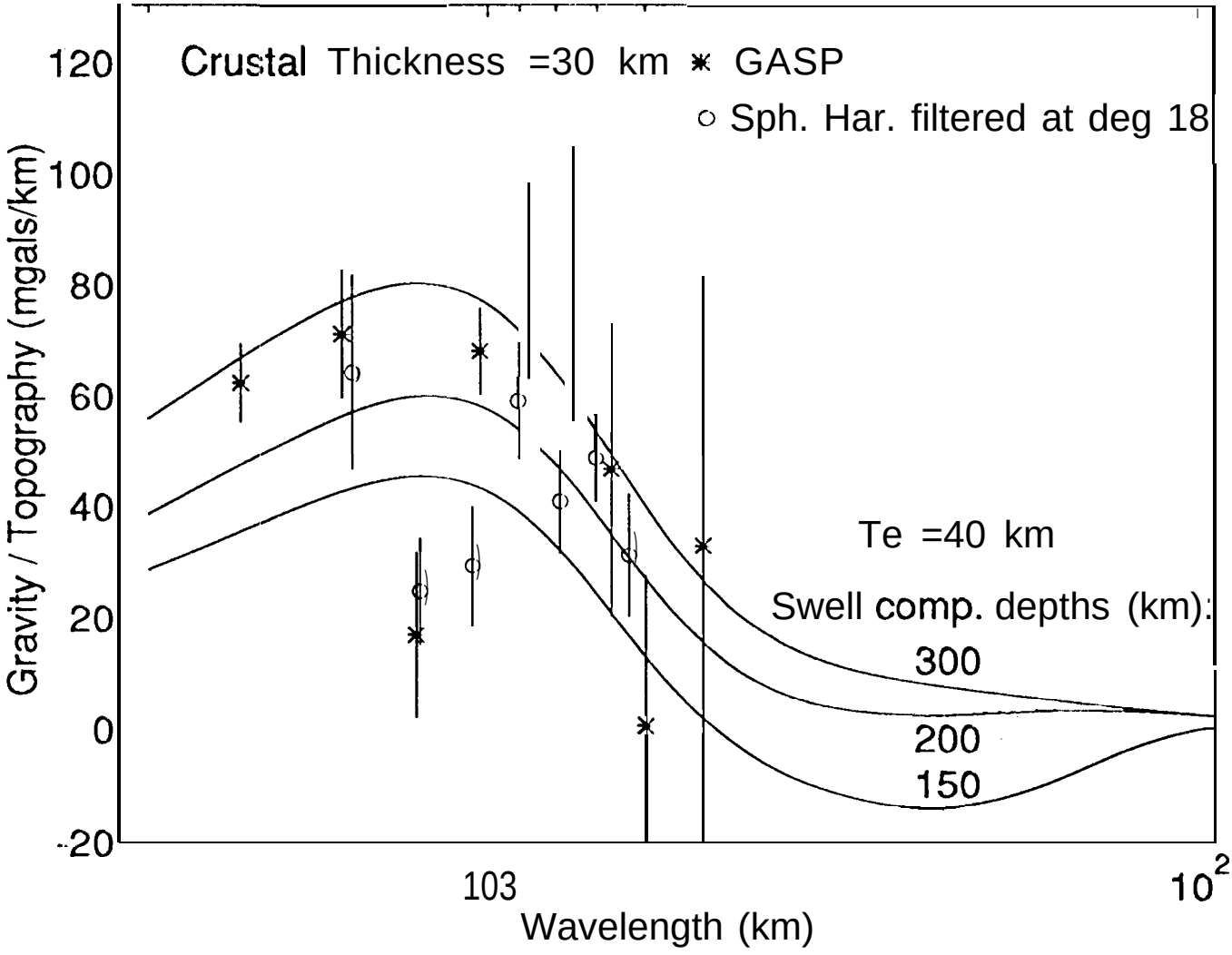
Crustal Thickness =30 km * GASP
○ Sph. Har. filtered at deg 18
Te =40 km
Swell comp. depths (km):
300
200
150
120
100
80
60
40
20
0
-20
Gravity / Topography (mgals/km)
103
10^2
Wavelength (km)

Figure 13C

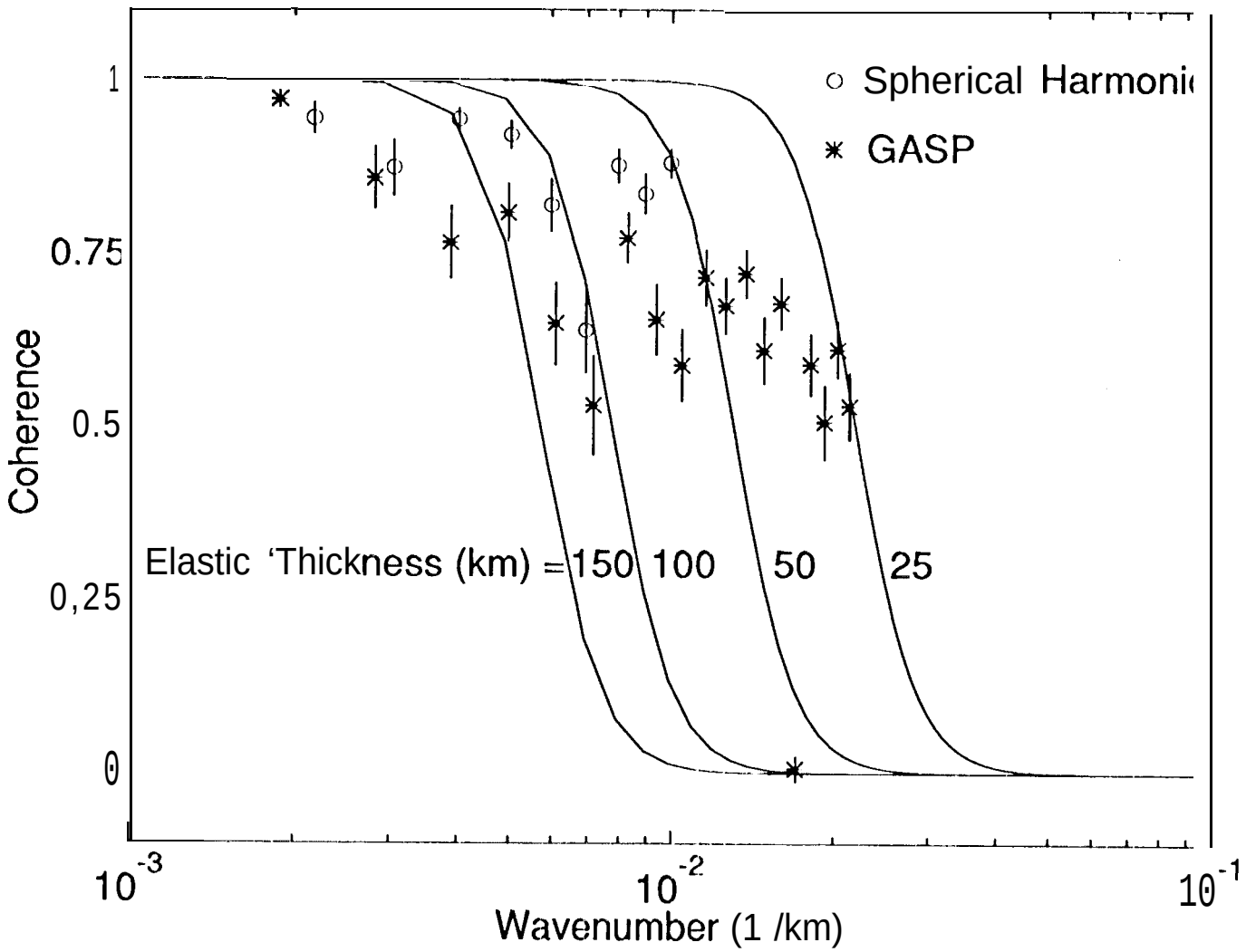
1
0.75
0.5
0,25
0
Coherence
Spherical Harmoni
GASP
Elastic 'Thickness (km) = 150 100 50 25
10^-3
10^-2
10^-1
Wavenumber (1 /km)

Figure 13d